Rapid volumetric brain changes after acute psychosocial stress

Uhlig, Marie [1,2]; Reinelt, Janis D. [1]; Lauckner, Mark E. [1,3,11]; Kumral, Deniz [1,4]; Schaare, H. Lina [1,5,6]; Mildner, Toralf [7]; Babayan, Anahit [1,8]; Engert, Veronika [9,10]; Villringer, Arno [1,8]; Gaebler, Michael [1,8]

[1] Department of Neurology, Max Planck Institute for Human Cognitive and Brain Sciences, Leipzig, Germany

[2] International Max Planck Research School NeuroCom, Leipzig, Germany

[3] Independent Research Group “Adaptive Memory”, Max Planck Institute for Human Cognitive and Brain Sciences, Leipzig, Germany

[4] Institute of Psychology, Neuropsychology, University of Freiburg, Freiburg im Breisgau, Germany

[5] Otto Hahn Group “Cognitive Neurogenetics”, Max Planck Institute for Human Cognitive and Brain Sciences, Leipzig, Germany

[6] Institute of Neuroscience and Medicine (INM-7: Brain and Behaviour), Research Centre Jülich, Germany

[7] NMR Group, Max Planck Institute for Human Cognitive and Brain Sciences, Leipzig, Germany

[8] MindBrainBody Institute at the Berlin School of Mind and Brain, Faculty of Philosophy, Humboldt-Universität zu Berlin, Berlin, German

[9] Institute of Psychosocial Medicine, Psychotherapy and Psychooncology, Jena University Hospital, Friedrich-Schiller University, Jena, Germany

[10] Independent Research Group “Social Stress and Family Health”, Max Planck Institute for Human Cognitive and Brain Sciences, Leipzig, Germany

[11] Medical Faculty of Leipzig University, Leipzig, Germany

Abstract (currently 212 of 250 words max.)

Rapid structural brain plasticity after acute stress has been shown in animals. It is unknown whether such stress-related brain changes also occur in humans, in which they have been found, using structural magnetic resonance imaging (MRI), after motor learning and visual stimulation. We here investigated grey matter volume (GMV) changes after acute stress in humans and tested their relation to psychophysiological stress measures.

Sixty-seven healthy men (25.8±2.7 years) completed a standardized psychosocial laboratory stressor (Trier Social Stress Test) or a control version while blood, saliva, heart rate, and psychometrics were sampled. T1-weighted MP2RAGE images at 3T MRI were acquired 45 min before and 90 min after intervention onset. GMV changes were analysed using voxel-based morphometry. Associations with endocrine, autonomic, and subjective stress measures were tested with linear models.

We found significant group-by-time interactions in several brain clusters including anterior/mid-cingulate cortices and bilateral insula: GMV was increased in the stress group relative to the control group, in which several clusters showed a GMV decrease. We found no significant group-by-time interaction for other MRI parameters, including cerebral blood flow, but a significant association of GMV changes with state anxiety and heart rate variability changes.

In summary, we show rapid GMV changes following acute psychosocial stress in humans. The results suggest that endogenous circadian brain changes are counteracted by acute stress and generally emphasize the influence of stress on the brain.

Keywords (7)

Humans, Magnetic Resonance Imaging, Brain, Autonomic Nervous System, Stress, Psychological, Neuroplasticity

Introduction

A stressor is a real or imagined threat to an organism's integrity or well-being, which elicits a psychological and physiological stress response (Herman et al., 2003). Rapidly activated and rapidly terminated, the stress response is highly adaptive in situations of acute threat, but a chronically activated stress system can have detrimental effects and constitutes a major risk factor for physical and mental disease (McEwen & Gianaros, 2010). While the stress response is orchestrated by the brain, it involves the whole organism, particularly the autonomic nervous system and endocrine systems, with the hypothalamic-pituitary-adrenal axis (HPA axis) as a central component (Kemeny, 2003). In turn, brain structure and function can be affected by stress, and rapid structural brain plasticity after acute stress has been shown in animals (Kassem et al., 2013). In the current study, we investigated rapid stress-induced brain changes in humans with structural magnetic resonance imaging (MRI).

The stress response comprises a cascade of hormonal signals including corticotropin-releasing hormone (CRH), vasopressin, adrenocorticotropic hormone (ACTH), and cortisol (Tsigos & Chrousos, 2002), which activates bodily functions to counteract the stressor. Most importantly, it triggers suppression of the immune system, faster glucose metabolization, and increased blood pressure (Cohen et al., 1991; Nesse et al., 2016). Being lipophilic, cortisol can cross the blood-brain barrier and, through its action on brain structures such as the hippocampus, terminate the stress response (Tasker & Herman, 2011; Joëls et al., 2013). This highlights the strong association of cortisol with long-term effects of stress on brain plasticity (McEwen & Gianaros, 2011), which occurs predominantly in regions involved in HPA axis regulation, such as prefrontal cortex (PFC), hippocampus, and amygdala (McEwen & Gianaros, 2011). Brain plasticity describes the brain's capacity to alter its structure and function to adapt to changing demands (Lövdén et al., 2010). Brain structure and function are thereby

inseparable, with structure constraining function and function shaping structure: In a supply-demand model, regional volume changes represent a continuous adaptation of the brain in supply (e.g., brain tissue) to changing environmental demands, mediated by alterations in activity (Lövdén et al., 2013). In support of this model, MRI studies often report a parallel development of structural and functional networks (He et al., 2007).

Stress-induced functional brain changes have been shown using MRI: During stress, the BOLD signal increased in prefrontal areas (Dedovic et al., 2009; Wheelock et al., 2016) and decreased in subcortical regions, including the hippocampus (Dedovic et al., 2009; Pruessner et al., 2008). Such stress-related brain changes in the PFC and subcortical regions also outlasted the stress task, which was ascribed to sustained vigilance or emotional arousal (Wang et al., 2005). Stress-related changes in functional connectivity have been shown in the salience network (Hermans et al., 2014), including the anterior cingulate cortex (ACC) and other cortical midline structures (Veer et al., 2011). These stress-related functional connectivity changes also correlated with individual cortisol trajectories (Veer et al., 2012). Analysing the resting-state fMRI from the experiment presented here, we previously found a stress-related increase in thalamic functional connectivity, which was linked to subjective stressfulness (Reinelt et al., 2019).

The link between chronic stress and structural brain changes in humans has been well-established (for a review see Radley et al., 2015): For example, stress-related psychopathologies have been associated with structural plasticity mainly in limbic and prefrontal areas (McEwen, 2005). Patients with post-traumatic stress disorder (PTSD) showed decreased GMV in the hippocampus (Chen et al., 2006; Karl et al., 2006), amygdala and ACC (Karl et al., 2006; Rogers et al., 2009). Also without a clinical diagnosis, higher levels of self-reported chronic stress have been associated with lower grey matter volume (GMV) in the hippocampus, amygdala, insula, and ACC (Ansell et al., 2012b; Lotze et al., 2020; Papagni et al., 2011).

In animal models, rapid stress-induced structural changes that have been detected within hours after acute stress exposure include attenuation of neurogenesis (marmosets: Gould et al., 1998, rats: Heine et al., 2004), changes in astrocyte density (in degus; Braun et al., 2009) or decreases in dendritic spine density (in mice; Chen

et al., 2010). In the latter study, a mediating function of the HPA axis in stress-induced memory deficits and associated brain structural changes was suggested.

Thus, while animal studies have found rapid structural brain changes after acute stress, these have - to our knowledge - not been shown in humans. We here used the Trier Social Stress Test (TSST, Kirschbaum et al., 1993), a strong and naturalistic psychosocial stressor in humans (Kirschbaum et al., 1993), and MRI to investigate structural brain plasticity.

In humans, structural brain changes are typically investigated using voxel-based morphometry (VBM; Ashburner & Friston, 2000; Draganski et al. 2004), which uses computational tissue classification based on T1-weighted images to detect differences in brain tissue composition. Numerous VBM studies have found rapid and spatially specific brain plasticity in response to exogenous stimuli such as training paradigms: for example, increased GMV in the motor cortex was found after one hour of balance training (Taubert et al., 2016) and after one hour of brain-computer-interface training in targeted brain regions (Nierhaus et al., 2021). Even after less active interventions, such as ten minutes of high-frequency visual stimulation (Naegel et al. 2017), or 263 seconds of passive image viewing (Månsson et al. 2020), GMV changes were found with VBM.

The physiology behind VBM-derived GMV changes remains unclear[1]. Theoretically, genesis of neurons, glia cells and synapses as well as vascular changes could underlie structural MRI changes in GM (Zatorre et al., 2012). Supporting findings with stressful interventions (mentioned above; Chen et al., 2010; Braun et al., 2009), animal studies that combined MRI and histological examination after training interventions have suggested neural dendrites and astrocytes as drivers of rapid, experience-induced brain changes in structural MRI (Keifer et al., 2015; Sagi et al., 2012). Both can occur after minutes to hours (Johansen-Berg et al., 2012).

Not only interventions but also endogenous changes at different time scales can affect measures of GMV: Ageing is a strong predictor for GMV decreases (Karch et al., 2019), but rhythmic GMV changes have also been reported over the course of the menstrual cycle and its hormonal fluctuations (Barth et al., 2016; Lisofsky et al., 2015)

[1] While we use the term “grey matter volume” for VBM changes, we consider it a placeholder, as other physiological changes may contribute to the signal (see below).

or with the circadian rhythm (Karch et al., 2019; Nakamura et al., 2015; Orban et al., 2020; Trefler et al., 2016). Total GMV decreased linearly from morning to afternoon in several studies (Karch et al., 2019; Nakamura et al., 2015; Trefler et al., 2016), particularly in medial prefrontal areas and the precuneus (Trefler et al., 2016). In addition, CSF increased over the course of the day (Trefler et al., 2016) whereas total white matter decreased in one study (Trefler et al., 2016), but was not associated with time of day in another (Karch et al., 2019). The circadian system and the stress system both maintain homeostasis by adapting to environmental conditions, and they strongly interact on the physiological level with the HPA axis, which is a major component of both systems (Nader et al., 2010; Nicolaides et al., 2014).

Rapid GMV changes may also occur with alterations in the participant's physiological state during MRI, for example by changes in hydration (Streitbürger et al., 2012) or osmolality (Höflich et al., 2017; Streitbürger et al., 2012). Furthermore, vascular changes can impact VBM results, because blood and GM have similar T1 relaxation values at 3T (Tardif et al., 2017; Wright et al., 2008), and changes in blood oxygenation and tissue oxygenation (Tardif et al., 2017) or cerebral blood flow (CBF; Franklin et al., 2013; Ge et al., 2017) may "masquerade" as changes in VBM-derived GMV. To specify the stress-related structural plasticity found with VBM and clarify the contribution of vasculature, we complemented VBM with other MRI measures: CBF measured with pulsed arterial spin labeling (pASL) and quantitative T1. An increase in T1 values would be consistent with a shift towards T1 values of blood and has been discussed as an increase in vascular tissue in the context of training-induced plasticity (Thomas et al., 2018). On the other hand, increased oxygenation following a breathing challenge has been shown to decrease T1 values (Tardif et al., 2017), which has been ascribed to the so-called tissue oxygenation-level dependent (TOLD) contrast (Haddock et al. 2013). To investigate differences between T1 maps, T1-weighted images and (preprocessed) VBM images, we also analysed intensity values from (unpreprocessed) T1-weighted (UNI) images within the VBM clusters.

To summarize, rapid GMV changes have been detected in humans upon exogenous stimulation and with endogenous fluctuations, and in animals following stress exposure. We hypothesized that acute stress, as a relevant exogenous stimulus triggering an endogenous process (i.e., the stress response), can induce rapid

changes in GMV measured with MRI. To test this hypothesis, we had young, healthy men complete either a psychosocial stress test (Trier Social Stress Test, TSST; Kirschbaum et al., 1993) or a closely related control intervention without a psychosocially stressful component (Placebo-TSST; Het el al., 2009). Before and after the intervention, we acquired MRI data. Throughout the entire experiment, we regularly sampled autonomic, endocrine, and subjective markers of the stress response (Figure 1).

As stress-induced brain changes have often been reported in the amygdala and the hippocampus (see above), they served as regions-of-interest (ROIs), complemented by an exploratory whole-brain analysis. To better depict the physiology of stress-induced brain changes, we also compared CBF and quantitative T1 values before and after the intervention. Additionally, we investigated the relation between GMV changes and the other (i.e., autonomic, endocrine, and subjective) stress measures.

Methods

Participants

We recruited male participants between 18 and 35 years of age via leaflets, online advertisements, and the participant database at the Max Planck Institute for Human Cognitive and Brain Sciences in Leipzig. Exclusion criteria, as assessed in a telephone screening, were smoking, excessive alcohol / drug consumption, past or current participation in psychological studies, regular medication intake, history of cardiovascular or neurological diseases, and a BMI higher than 27. In addition, standard MRI exclusion criteria applied, such as tattoos, irremovable metal objects (e.g., retainers, piercings), tinnitus, and claustrophobia.

We tested 67 young, healthy males. Because of an incidental medical finding, one participant was excluded, so that 66 participants (age: 25.8 ± 2.7, 21-32 years) entered the analyses, 32 in the stress and 34 in the control group.

On separate days prior to the stress/control paradigms, participants underwent extensive baseline measurements that included cognitive testing, blood screening, anthropometrics, structural and resting-state functional MRI scans, resting-state

electroencephalography (EEG), self-report questionnaires, and a structured clinical interview (for details, see Babayan et al., 2019). If exclusion criteria were detected during the baseline assessment, participants were excluded from further testing. Included participants were randomly assigned to either the stress or the control group. To avoid experimenter biases, the administrative staff remained blind to the testing condition until the first MRI session. All appointments were scheduled for the same time of day (11:45 am) to control for diurnal fluctuations of hormones (e.g., cortisol and ACTH; Nader et al., 2010; Nicolaides et al., 2014). Participants were asked to sleep at least 8 hours in the night before the experiment, to get up no later than 9 am, have a normal breakfast and to not eat or exercise until their study appointment while also refraining from drinking coffee, black tea, or other stimulant drinks. Written informed consent was obtained from all participants. The study was approved by the ethics committee of the medical faculty at Leipzig University (number 385-1417112014), and participants were financially compensated.

Stress and the control groups did not differ significantly in age, hours of sleep on the day of testing, average sportive activity per week, or self-reported chronic stress (Reinelt & Uhlig et al., 2019).

Procedure

The pre-scan was completed on average 45 (SD: ±3.9) min before intervention onset (before two resting-state fMRI scans, see Figure 1), and the post-scan was completed on average 88 (SD: ±3.6) min after intervention onset (between four resting-state fMRI scans, see Figure 1).

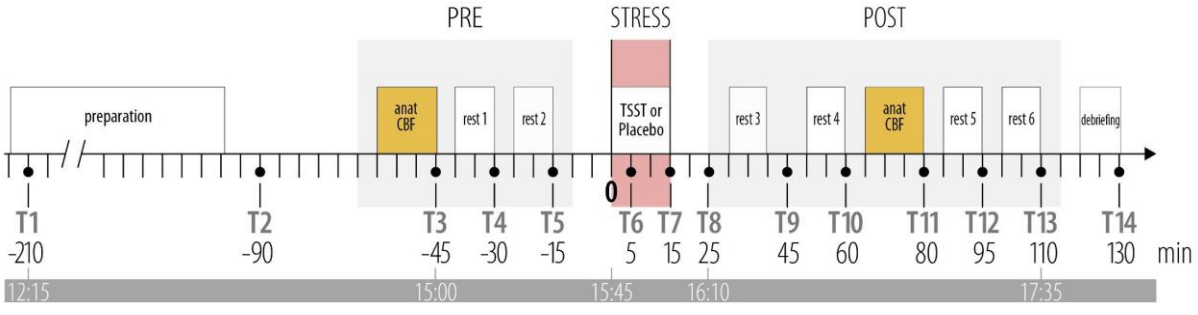

Figure 1. Schematic overview of the experiment: Between-subject design with the stress group (n = 33) undergoing the Trier Social Stress Test (TSST) and the control group (n = 34) a placebo-TSST. Orange boxes indicate two anatomical scans (anat) using T1-weighted MRI (MP2RAGE) and two scans of pulsed arterial spin labelling for cerebral blood flow (CBF).

Psychometric ratings, saliva samples, and blood samples were acquired at 14 time points throughout the experiment (T1-T14). Minutes are relative to the onset of the intervention (TSST or placebo-TSST), while the bottom bar informs about the time-of-day. The grey boxes indicate phases in the MRI. (The TSST and the placebo-TSST took place outside of the MRI.)

Intervention

Each participant completed either a psychosocial stress test (Trier Social Stress Test, TSST; Kirschbaum et al., 1993) or the placebo-TSST as control intervention, which tightly controls for physical and cognitive load during the TSST (Het et al., 2009).

Participants in the stress group prepared for (5-min) and completed a job interview (5-min) as well as a difficult mental arithmetic task (5-min) in front of a committee (one female, one male professional actor), introduced as two professional psychologists trained in the analysis of nonverbal communication. Additionally, the task was recorded by a video camera and microphone. In the control condition, participants prepared (5-min) and spoke about their career aims (5-min) and solved an easy mental arithmetic task (5-min) with nobody else in the room and no video or audio recording. To extend the stressfulness of the TSST, participants in the stress group were told that a second task would follow during the scanning procedure. To make this scenario more plausible, participants were brought back to the scanning unit in the company of the experimenter *and* the TSST committee members. Only after rest 4, before the anatomical scan (+60 min after TSST onset), they were told that no additional task would follow. For a more detailed description of the interventions, see supplementary material and Reinelt & Uhlig et al. (2019).

Throughout the experiment, blood was sampled at 14 time points, and saliva and subjective ratings at 15 time points. At each sampling point, participants completed psychometric questionnaires, while autonomic and endocrine data were acquired. For further details, see below as well as Reinelt & Uhlig et al. (2019) and Bae & Reinelt et al. (2019).

Magnetic resonance imaging

Acquisition

MRI was performed on a 3T MAGNETOM Verio (Siemens AG, Erlangen, Germany) scanner with a 32 channel Siemens head-coil. The MP2RAGE sequence was used to acquire structural MR images. The MP2RAGE sequence yields a nearly bias-free T1-weighted (UNI) image, which is created by combining the two inversion images (INV1, INV2) and it produces a quantitative T1 map (T1) (Marques et al., 2010). The high-resolution MP2RAGE sequence had the following parameters (Marques et al., 2010): TI1 = 700 ms, TI2 = 2500 ms, TR = 5000 ms, TE = 2.92 ms, FA1 = 4°, FA2 = 5°, 176 slices, voxel dimensions = 1 mm isotropic.

Cerebral blood flow (CBF) was measured using the pulsed arterial spin labeling (pASL) sequence from Siemens (PICORE). For a detailed description of the pASL data acquisition, preprocessing, analysis and results, see supplement.

Preprocessing

VBM: For each scan (pre-intervention, post-intervention), a brain mask was created from the INV2-images to remove the noisy background of the UNI images, which is a by-product of the division of the two inversion images. These denoised T1-weighted images were preprocessed using the longitudinal preprocessing pipeline (with default settings, Version 1450 (CAT12.6) 2019-04-04) of the CAT12 toolbox (http://www.neuro.uni-jena.de/cat/) including intra-subject realignment, bias correction, segmentation, spatial registration to MNI space, segmentation into three tissue types (grey matter, white matter, and cerebrospinal fluid). Finally, the images were smoothed with a Gaussian kernel at 8 mm full-width at half maximum (FWHM). For further analysis, the segmented grey matter images were used.

T1 & T1-weighted: The denoised T1-weighted images were warped to MNI-space (using the *normalize:estimate&write* function in SPM). T1 maps were normalized to MNI space by applying the deformations from the normalization of the T1-weighted images. The normalized T1-weighted and T1 images were masked with the same sample-specific GM mask, which was used for the VBM-analysis before smoothing with an 8-mm FWHM Gaussian kernel.

CBF: PASL data was preprocessed using an inhouse Matlab analysis pipeline, which included motion correction with linear regression. Images were realigned with FSL *McFlirt* and smoothed with a 2D spatial Gaussian filter of 3-mm FWHM (for details, see supplement).

Postprocessing

For post-hoc analyses (see below for details), significant ($p_{FWE}<0.05$) VBM clusters were saved as binarized NIfTI images from the result GUI and used as masks for post-hoc tests and to investigate changes in T1 and T1-weighted intensity values as well as CBF. For binarizing masks, multiplication with masks and extraction of GMV, T1 and T1-weighted intensity values, FSL was used (*fslmaths* & *fslstats* in *fslutils*, (Jenkinson et al., 2012).

VBM post-hoc: GMV values were extracted by multiplying binary masks of VBM clusters with the smoothed, preprocessed GM images and extracting the average value from each cluster.

T1 & T1-weighted: Values were extracted by multiplying binary masks of VBM clusters with the smoothed and normalized T1 and T1-weighted images and extracting the average value from each cluster. Additionally, average values from GM voxels outside of the VBM clusters were extracted to serve as a reference for potential global changes in T1 values or T1-weighted intensity values. Therefore, the smoothed, GM masked images were multiplied with an inverse binary VBM-cluster mask.

CBF: For the CBF analysis, the masks were resampled to a 2-mm isotropic voxel size to match the pASL images using the *coregister:reslice* function in SPM12. The preprocessed CBF maps were multiplied with binary masks for VBM clusters and the average CBF value for each cluster was extracted. As the pASL data is acquired within a manually defined slab, not all VBM clusters were fully covered (see Figure S1). Only clusters, in which CBF data was available for at least 70% of voxels were included in the post-hoc CBF analysis.

Anatomical regions-of-interest definition

To test our regional hypotheses, anatomical regions-of-interest (ROIs) were created as binary masks of hippocampus and amygdala using the Anatomy toolbox (Eickhoff

et al., 2005) and resampled to 1.5-mm space using SPM12 to match the anatomical images. ROI values were extracted by multiplying masks with the smoothed, modulated, warped, coregistered images using FSL (*fslmaths* & *fslstats* in *fslutils*, Jenkinson, et al., 2012). Below, “Hippocampus” and “Amygdala” (with capitalized first letters) refer to these anatomical ROIs.

Quality assessment

Image quality was assessed using the noise-to-contrast ratio (NCR), a quality parameter computed by the CAT12 toolbox from noise, bias and white-matter hyperintensities. Based on within-sample comparisons, data from participants whose image quality (NCR) was more than 3 standard deviations (SD) below the sample mean were excluded (see supplementary material). Systematic changes in image quality were tested with a linear mixed model, which showed a significant group-by-time interaction effect for NCR ($X^2(1)=7.9$; $p=0.0049$; see supplement), driven by a significant decrease in image quality in the control group (t-ratio=3.3, p=0.0016). Head movement can negatively influence image quality in MRI (Power et al., 2015) as well as estimates of GMV and cortical thickness (Reuter et al., 2015). As no information about head movement was available from the MP2RAGE data, we calculated mean framewise displacement (MFD) as the sum of the absolute values of the six realignment parameters (Power et al., 2015) from the resting-state fMRI scans that directly preceded the MP2RAGE scan. Accounting for head motion by including MFD into the above model weakened the group-by-time interaction effect for NCR ($X^2(1)=3.7$; $p=0.059$). Furthermore, a non-significant trend for an effect of MFD on NCR ($F(1)=3.4$, $p=0.068$) was found, suggesting an association between the two quality parameters. To avoid circular analyses (since NCR was derived from the data), we included MFD in our statistical models to account for quality changes on volume estimates.

For extracted T1 and T1-weighted intensity values, values outside the range of 3 SD above sample mean were excluded (for details, see respective section below).

The quality assessment of CBF data is described in the supplement.

Psychophysiological stress measures

Autonomic

Heart rate (HR) and heart rate variability (HRV) were analysed from recordings of electrocardiography (ECG) and photoplethysmography (PPG). A detailed description of autonomic data acquisition and data preprocessing can be found in Reinelt & Uhlig et al. (2019). Autonomic recordings were binned into three-minute intervals. The average interbeat interval (the inverse HR) was determined for each interval and HRV was quantified as the square root of the mean squared differences of successive differences (RMSSD) in interbeat intervals, indexing parasympathetic cardio-regulation (e.g., Malik et al., 1996).

Endocrine

Saliva was sampled with a Sarstedt Salivette (Sarstedt, Nümbrecht, Germany) for at least 2 min per sample. Blood samples (serum and plasma; Sarstedt Monovette) were acquired by the experimenter from a intravenous catheter in the left or right cubital vein. Saliva and blood samples were analysed using Liquid chromatography-tandem mass spectrometry (LC-MS/MS) at the Institute for Laboratory Medicine, Clinical Chemistry and Molecular Diagnostics, University of Leipzig, following the protocol described in (Gaudl et al., 2016). Saliva cortisol and plasma ACTH were used to assess the association of GMV changes with endocrine stress measures at different times of HPA axis activation: ACTH, which is secreted earlier during HPA axis activation, peaked at 15 min after stressor onset, while saliva cortisol, a particularly robust stress marker (Vining et al., 1983), peaked at 25 min after stressor onset. A detailed analysis of changes in endocrine markers and their timing in the current study can be found in (Bae et al., 2019). Participants with a cortisol increase below 1.5 nmol/l following psychosocial stress exposure can be considered non-responders and are often excluded from analyses including endocrine data (Miller et al., 2013).

Subjective

We presented questionnaires with OpenSesame 3.1.2 (Mathôt et al., 2012) on a laptop (outside MRI) or on a screen (inside MRI). Participants answered the questions with two keys on the laptop keyboard (outside MRI) or with a button box (inside MRI). For

this analysis, subjective stress was assessed with the state trait anxiety questionnaire (STAI, sum score of the state subscale; (Laux, 1981; Laux & Spielberger, 2001) and the individual stressfulness question “How stressed do you feel right now?”, which was answered using a visual analogue scale (VAS) with a sliding bar from 0 (“not at all”) to 100 (“very much”).

Statistical Analysis

Analysis of neuroimaging data

Whole-brain analysis in SPM

Following quality assessment, three participants (two in the stress group) were excluded from the VBM analysis because of an NCR value more than 3 SD below the sample mean. The final VBM sample therefore consisted of 63 participants, 30 in the stress group and 33 in the control group. For statistical analysis of the MRI data, delta images were created by subtracting the pre-intervention image from the post-intervention image. A two-sample t-test was performed on the difference images to investigate the group-by-time interaction. To focus the analysis on GM, thresholding is typically used in VBM analyses (e.g. Streitbürger et al., 2012). Since the voxel values in delta images describe a difference rather than the tissue probability itself, they could not be thresholded. Instead, we used a sample-specific GM mask. This mask is automatically created during model estimation in SPM; in our case a one-sample t-test on all smoothed, segmented GM images while applying an absolute masking threshold of 0.1 (probability of this voxel being GM).

The total intracranial volume (TIV) was estimated for both images (pre-intervention, post-intervention) of each subject using CAT12 and their average was included as a covariate. To account for potential systematic, group-specific changes in image quality (see the section “Quality assessment” above and supplement), MFD was included as a proxy for head motion as an additional covariate. The results from the two-sample t-test on Δgrey matter images (ΔGM) were investigated using two-sided t-contrasts (i.e., control>stress [1 -1 0 0] and control<stress [-1 1 0 0] with TIV and MFD in columns 3 and 4).

To minimize false positive and false negatives results, we used whole-brain threshold-free cluster enhancement (TFCE), a non-parametric multiple-comparison correction that does not require a cluster extent threshold, using the TFCE-toolbox (http://dbm.neuro.uni-jena.de/tfce) with the default settings of 5000 permutations and the Smith-permutation method. Anatomical labels for significant clusters were found using the DARTEL-based "neuromorphometrics atlas" provided with the CAT12 toolbox. Below, we use capitalization to indicate the extracted anatomical labels (e.g., "Superior Medial Frontal Gyrus")

Analysis of extracted imaging markers

Statistical analysis at the ROI level was performed using R 3.0.2 (R Core Team (2013); http://www.R-project.org/). Group differences in variables-of-interest over time were investigated with linear mixed models (LMMs; using the *lme4* package; (Bates et al., 2015), which included a random intercept for each subject to account for inter-individual differences. Visualizations were created in R using *ggplot* (Wickham, 2009). The raincloud plots were adapted (Allen et al., 2019).

Linear mixed model design

Across all analyses, the model was built following the same procedure (the full scripts can be found on https://gitlab.gwdg.de/necos/vbm.git):

1. A null model including a random intercept, covariates of no interest, as well as reduced fixed effects was set up and compared to a full model (Forstmeier & Schielzeth, 2011).
2. The full model was identical to the null model except for the effect of interest, in most cases the group-by-time(-by-cluster) interaction or other (i.e., autonomic, endocrine, or subjective) stress measures when testing their associations with GMV.
3. The difference between the full and the null model was tested using the *anova* function and setting the argument *test* to "chisq" to do a X^2 (Chi^2) test.
4. The *drop1* function was used to extract the results from the individual effects.
5. Non-significant interactions were dropped from the full model to reduce complexity (reduced model).

6. In case of significant interactions, the effects at the individual levels of predictors (e.g., within-group or for each cluster) were analyzed post-hoc using the *emmeans & contrast* function with *Holm* correction from the *emmeans* package (Lenth, 2021). Estimated marginal means and 95% confidence intervals obtained with *emmeans* were used for plotting.

We tested the assumptions for LMMs by visually inspecting the distribution of residuals in a QQplot and a scatterplot of the residuals plotted against fitted values. The main criterion for the latter was symmetry along the y-axis. Influential cases were identified and excluded. Multicollinearity was tested by extracting the variance inflation factor (VIF), using the *vif* function in the *car* package (Fox & Weisberg, 2018). To increase the likelihood of symmetrically distributed residuals, distribution of all variables was estimated visually using histograms, and data was transformed (default: natural logarithm) when data distribution appeared asymmetrical. The covariate MFD was also log-transformed and both covariates of no interest, TIV and $\log_e$(MFD) were z-transformed to increase interpretability of the results (Schielzeth, 2010).

Post-hoc analysis of VBM results: Post-hoc analysis in significant VBM clusters was performed to confirm SPM analyses, in which the 2-by-2 design (group-by-time) was reduced to a two-sample t-test over the difference images (post- minus pre-intervention). The full model included the main effects, all two-way interactions, and the three-way interaction of group, time, and cluster (plus covariates $\log_e$(MFD) and TIV), while the null model lacked all interactions. GMV values were square-root transformed. If the three-way interaction was not significant, it was excluded from the full model (reduced model).

In addition to the “global” model including all clusters, group-by-time interaction effects were additionally tested in “local” models for each cluster separately, which allowed the investigation of regional differences and patterns. Since the effect of interest here was the group-by-time interaction effect, the null model only included the main effects of group and time as fixed effects. The model equation is depicted below; $\beta_{3\ldots}\,\beta_7$ denotes all two-way interactions and the main effects of all variables in interaction terms, *u* and *e* depict random intercepts per subject and subject residuals.

The GMV values from the individual clusters were $\log_e$-transformed. The *p* values from the full-null-model comparison were corrected using the *Holm-Bonferroni* method in the *p.adjust* function from the *stats* package.

Following a significant group-by-time interaction effect, post-hoc tests were conducted to test within-group effects using the *emmeans* function with *Holm-Bonferroni* correction from the *emmeans* package (Lenth, 2021).

Full model:

$$\sqrt{GMV} \sim \beta_0 + \beta_1(Group \times Time \times Cluster) + \beta_2(Group \times Time) + \beta_3(\dots)\,\beta_7 + \beta_8 log_e(MFD) + \beta_9(TIV) + u_{subject} + \varepsilon_{subject}$$

Reduced model:

$$\sqrt{GMV} \sim \beta_0 + \beta_1(Group \times Time) + \beta_2(Cluster \times Time) + \beta_3(Group) + \beta_4(Time) + \beta_5(Cluster) + \beta_6 log_e(MFD) + \beta_7(TIV) + u_{subject} + \varepsilon_{subject}$$

Null model:

$$\sqrt{GMV} \sim \beta_0 + \beta_1(Group) + \beta_2(Time) + \beta_3(Cluster) + \beta_6 log_e(MFD) + \beta_7(TIV) + u_{subject} + \varepsilon_{subject}$$

Total GM, total WM, and CSF:

Only data of participants included in the VBM analysis were used.

Log-transformation was applied to values of total GM and total WM, while total CSF was left untransformed. The full models included the main effects and the group-by-time interaction (plus covariates $\log_e$(MFD) and TIV), while the null models lacked the interaction. Significant interaction effects were followed by post-hoc tests using the *emmeans* function.

Quantitative T1 values: Only data of participants included in the VBM analysis were used.

Before analysis, T1 values were z-transformed and outliers of 3 SD below the sample mean were removed. Because 11 of the resulting 13 outliers came from the same two participants, these were excluded from the T1 analysis entirely (remaining sample: n=61). For the "global" model, T1 values were left untransformed (criterion: symmetry of the distribution of residuals; see above). The full model included the main effects, all two-way interactions, and the three-way interaction of group, time, and cluster (plus covariates $\log_e$(MFD) and TIV), while the null model lacked all interactions. If the three-way interaction was not significant, it was excluded from the full model (reduced model). The null model remained unchanged. Significant interaction effects were followed by post-hoc tests using the *emmeans* function.

T1-weighted intensity values: Only data of participants included in the VBM analysis were used.

Before analysis, T1-weighted intensity values of 3 SD above the sample mean were excluded as outliers. Since the resulting 6 outliers came from the same participant, he was excluded from the analysis (analysed sample: n=62). The full model included the main effects, all two-way interactions, and the three-way interaction of group, time, and cluster (plus covariates $\log_e$(MFD) and TIV), while the null model lacked all interactions. In the "global" model, T1-weighted intensity values followed a symmetrical distribution and were left untransformed.

Anatomical ROIs: We investigated group differences in GMV over time within the hypothesized four ROIs in four separate models (left and right amygdala, left and right hippocampus). As the effect-of-interest was the group-by-time interaction, the null model only included main effects of group and time. GMV values were $\log_e$-transformed.

CBF changes in the VBM clusters and in the whole brain

Following quality assessment, three participants were excluded from the pASL analysis. To investigate the impact of group and time on CBF within the VBM clusters,

LMMs were set up in analogy to the VBM-ROI analysis. In addition to the factors group, time, cluster, and their interaction, a random effect per participant was included. The covariates TIV and MFD (included in the VBM-LMMs) were not included in the pASL analysis, because the preprocessing of the pASL data already included motion correction and TIV does not affect the intervention-induced change in CBF within a predefined region. (For a control analysis showing no significant effect of TIV, MFD or age on CBF data across all voxels from VBM clusters, see supplement).

As an exploratory analysis, group-specific CBF changes over time were assessed similarly to the VBM analysis, that is, groups were compared with a two-sample t-test on the difference images (post-pre) in SPM12. No nuisance variables were included, the sample-specific GM mask was used, and the threshold for TFCE correction was $p_{FWE}<0.05$.

Analysis of endocrine, autonomic, and subjective stress measures

We investigated changes in autonomic (HR, HRV), endocrine (saliva cortisol, plasma ACTH), and subjective stress measures (STAI - state anxiety, VAS “stressfulness”) over time between groups using LMMs. All time points beginning from directly after the first (T3) until directly after the second (T11) anatomical MR scan were included (10 time points). One “non-responder” participant was excluded from the endocrine analysis due to a cortisol increase below 1.5 nmol/l (Miller et al., 2013), another was identified as an influential outlier by visual inspection of the residuals plot and excluded from the saliva cortisol model. The full model included group and time as well as their interaction and baseline (mean between 2 time points before intervention) values as fixed effects and a random intercept per subject. Full models were compared against the respective null model lacking the interaction effect with X^2 tests. Saliva cortisol, plasma ACTH, HR, and STAI score values were $\log_e$-transformed, HRV and VAS stressfulness values were square-root transformed. (More details on LMM analysis can be found in the section *Analysis of extracted imaging markers* above.)

Association of VBM changes with other stress measures

We conducted two types of analyses to investigate the association of GMV changes with endocrine, autonomic, and subjective stress measures: LMMs were used to analyse the effect of the trajectory of endocrine, autonomic, and subjective stress

563 measures on GMV changes. Linear models (LMs) were used to test the association
564 between stress reactivity and GMV changes by analyzing the association of ΔGMV
565 values (post-pre) and the peak reactivity value of the stress measures (maximum-
566 baseline). Peak reactivity is commonly used in stress research (Engert et al., 2013;
567 Van Cauter & Refetoff, 1985), also to determine individuals with a cortisol increase
568 below physiological relevance ("non-responders"; Engert et al., 2013; Miller et al.,
569 2013; Van Cauter & Refetoff, 1985).

570 LMMs have the advantage of covering the trajectory of stress measures by including
571 data from all timepoints (before, during, and after the intervention). However, this high
572 number of observations in stress measures also adds a lot of variance compared to
573 GMV data, available at only two time points, which may overfit the model. Please note
574 that both LMMs and LMs (with Δ values) are complementary analyses, which - since
575 they are not built on the same data - cannot be directly compared with regard to
576 variance explained (e.g., adjusted R^2) or model fit (e.g., Akaike Information Criterion
577 AIC).

578 P values from LMMs and LMs were multiple comparison-corrected using Holm's
579 method (Holm, 1979; 6 stress measures, 2 analyses, LMM and LM, each = 12) as
580 implemented in the *p.adjust* function of the *stats* package. In case of significance, the
581 *emtrends* function from the *emmeans* package (Lenth, 2021) was used to extract the
582 within-group estimates and test for a significant interaction effect. The *drop1* function
583 was used to extract the estimates and *p* values for the single predictors.

584

585 *Association of VBM changes with other stress measures (LMMs)*: Stress measures
586 (saliva cortisol, plasma ACTH, HR, HRV, STAI score, and VAS score) were included
587 in separate full-model LMMs and tested against a null model without them. The model
588 equation is depicted below; $\beta_{3\ldots}\,\beta_7$denotes all two-way interactions and the main
589 effects of all variables in the interaction term, *u* and *e* depict random intercepts per
590 subject and subject residuals.

591

592

593

Full model:

$$\sqrt{GMV} \sim \beta_0 + \beta_1(Group \times Time \times StressMeasure) + \beta_2(Group \times Time) + \beta_3(\ldots)\,\beta_7 + \beta_8 Cluster + \beta_9 log_e(MFD) + \beta_{10}(TIV) + u_{subject} + \varepsilon_{subject}$$

Null model:

$$\sqrt{GMV} \sim \beta_0 + \beta_1(Group \times Time) + \beta_4 Cluster + \beta_5 log_e(MFD) + \beta_6(TIV) + u_{subject} + \varepsilon_{subject}$$

Association of ΔVBM with peak reactivity of other stress measures (LMs): ΔGMV values were calculated by subtracting the pre- from the post-scan value. Δ values of stress-measures (saliva cortisol, plasma ACTH, HR, HRV, STAI score, and VAS-score) were peak reactivity values calculated by subtracting the baseline value from the maximum value within 15-45 minutes after intervention onset (Engert et al., 2013; Van Cauter & Refetoff, 1985). The assumptions for LMs were tested as described above for LMMs.

ΔGMV was the dependent variable in all models. The full model included group and peak reactivity of stress measures as well as their interaction and the mean of pre- and post-TIV as well as MFD as independent variables. This was compared against a null model lacking the peak reactivity of stress measures using an F-test.

Full model:

$$\Delta GMV \sim \beta_0 + \beta_1(Group \times Peak\,reactivity) + \beta_2(Group) + \beta_3(Peak\,reactivity) + \beta_4(Cluster) + \beta_5(\underline{MFD}) + \beta_6(\underline{TIV})$$

Null model:

$$\Delta GMV \sim \beta_1(Group) + \beta_2(Cluster) + \beta_5(\underline{MFD}) + \beta_6(\underline{TIV})$$

Results

Analysis of neuroimaging data

Whole-brain VBM

After quality assessment, the VBM was analysed in 63 participants: 30 in the stress group (TSST) and 33 in the control group (placebo-TSST). The results from the two-sample t-test on Δgrey matter images (ΔGM) were investigated using two-sided t-contrasts (i.e., control>stress and control<stress). The T contrast for control>stress did not yield statistically significant results. The opposite contrast (control<stress] showed a significant (p_{FWE}<0.05) effect in 16 clusters (see Table 1, & Figure 2), including cortical midline structures (CMS) and bilateral insula. (The cluster with an extent of 1 voxel was excluded from further analyses).

The unthresholded results maps can be found at https://www.neurovault.org/collections/SFQXOIUB/.

Post-hoc LMMs in VBM clusters

The VBM GM values from the whole-brain analysis result clusters were extracted and the findings were tested in a post-hoc analysis using LMMs. The “global” model confirmed the significant group-by-time interaction effect across all clusters ($X^2(1)=6.12$, p=0.0133). The three-way interaction group-by-time-by-cluster was not significant ($X^2(46)=41.64$, p=0.6551), showing no evidence for significantly different group-by-time effects between clusters. The three-way interaction was thus removed from the model.

Post-hoc tests revealed a non-significant trend for a GMV decrease in the control group (-1.3%, β_c = -0.004, t/t(2020)= -2.09, p=0.0737) and no significant change in the stress group (+0.8%, β_s= 0.004, t/t(2007)= 1.50, p=0.1331).

In individual “local” models, the full-null-model comparison showed a significant group-by-time interaction effect in all 15 clusters tested (see Table 1 for details). Post-hoc tests revealed three patterns behind the interaction (Figure 2):

1) eight clusters, including the biggest cluster in the anterior cortical midline (Left Superior Medial Frontal Gyrus) and the Left Anterior Insula, showed a significant GMV decrease in the control group, and no significant change in the stress group;

2) four clusters, including the Right Angular Gyrus and Left Mid-Cingulate Cortex, showed a significant GMV increase in the stress group and no significant change in the control group; and

3) three clusters, including the Right Posterior Insula, showed both a significant GMV decrease in the control group and a significant GMV increase in the stress group.

	Hemis-phere	**Cluster Name**	**Cluster Size**	**p_{FWE} (TFCE)**	**x y z**	**Linear Mixed Model (Holm-Bonferroni-corrected)**	**Post-Hoc Test (Holm-Bonferroni-corrected)**	**Estimates [Pattern]**
1	L	Superior Medial Frontal Gyrus	2364	0.014	-03 50 30	$X^2(1)$= 9.1, p=0.0175	$t/t_c(66.5)$= -4.2, p= 0.0002 $t/t_s(68.6)$= 0.7 p= 0.4915	β_c =-0.013* β_s = 0.002 [1]
2	R	(posterior) Insula	2441	0.015	43 -12 04	$X^2(1)$= 14.3, p=0.0019	$t/t_c(66.5)$= - 3.8, p= 0.0007 $t/t_s(68.8)$= 2.2, p= 0.034	β_c=-0.011* β_s= 0.007* [3]
3	L	(anterior) Insula	466	0.027	-40 -08 06	$X^2(1)$= 11.3, p=0.0062	$t/t_c(66.5)$= - 4.3, p=0.0001 $t/t_s(68.3)$= 1.0 p= 0.3012	β_c =-0.014* β_s= 0.004 [1]
4	R	Angular Gyrus	696	0.035	54 -63 28	$X^2(1)$= 15.5, p=0.0011	$t/t_c(66.6)$= 0.0, p= 0.9845 $t/t_s(70.8)$= 5.6, p< 0.0001	β_c =0.0001 β_s= 0.038* [2]
5	L	Parahippo campal Gyrus	35	0.038	43 -12 04	$X^2(1)$= 17.4, p=0.0005	$t/t_c(66.5)$= 4.4, p< 0.0001 $t/t_s(68.7)$= 0.3, p=0.734	β_c =-0.029* β_s= -0.002 [1]
6	R	Inferior Occipital Gyrus	118	0.042	52 -80 03	$X^2(1)$= 12.6, p=0.0042	$t/t_c(66.6)$= -3.8, p= 0.0006 $t/t_s(71.2)$= 1.7, p=0.0919	β_c =-0.029* β_s= 0.015 [1]
7	L	Mid-Cingulate	160	0.042	-03 -24 46	$X^2(1)$= 8.2, p=0.0214	$t/t_c(66.5)$= 0.4, p= 0.7114	β_c =0.0001 β_s= 0.014* [2]

		Cortex					$t/t_s(68.5)$= 4.4, p= 0.0001	
8	R	Cerebro-Motor-Area	77	0.043	-04 -06 57	$X^2(1)$= 8.1, p=0.0214	$t/t_c(66.8)$= -1.5, p= 0.1307 $t/t_s(67.5)$= 2.7, p= 0.0193	β_c =-0.005 β_s= 0.009* [2]
9	R	Lateral Orbital Gyrus	79	0.045	36 39 -15	$X^2(1)$= 15.6, p=0.0011	$t/t_c(66.5)$= -3.3, p= 0.0031 $t/t_s(69.8)$= 2.7, p= 0.0091	β_c =-0.020* β_s= 0.019* [3]
10	R	Precuneus	141	0.046	03 -50 57	$X^2(1)$= 11.8, p=0.0052	$t/t_c(66.4)$= 0.4, p= 0.7201 $t/t_s(67.7)$= 5.2, p< 0.0001	β_c = 0.002 β_s= 0.026* [2]
11	R	Frontal Pole	52	0.046	24 63 03	$X^2(1)$= 8.9, p=0.0175	$t/t_c(66.4)$= - 4.8, p<0.0001 $t/t_s(68.3)$=-0.05, p= 0.9626	β_c =-0.021* β_s= -0.0002 [1]
12	R	Superior Medial Frontal Gyrus	44	0.047	06 52 04	$X^2(1)$= 16.6, p=0.0007	$t/t_c(67.0)$= -7.5, p< 0.0001 $t/t_s(67.4)$= -0.5, p= 0.5824	β_c =-0.019* β_s= -0.002 [1]
13	L	Superior Temporal Gyrus	48	0.048	-63 -10 04	$X^2(1)$= 12.4, p=0.0042	$t/t_c(66.5)$= - 2.9, p= 0.0088 $t/t_s(68.9)$= 2.4, p= 0.0193	β_c =-0.018* β_s= 0.017* [3]
14		//	1	0.048	51 -46 51	–	–	–
15	R	Middle Frontal Gyrus	22	0.048	45 46 12	$X^2(1)$= 8.1, p=0.0215	$t/t_c(66.4)$= -3.8, p= 0.0007 $t/t_s(68.1)$= 0.6, p= 0.5344	β_c = -0.016* β_s= 0.003 [1]
16	R	Middle Frontal Gyrus	23	0.050	42 54 -02	$X^2(1)$= 7.8, p=0.0215	$t/t_c(66.7)$= -3.7, p< 0.0009 $t/t_s(71.5)$= 0.7, p= 0.5177	β_c = -0.027* β_s= 0.005 [1]

Table 1. Results from VBM analysis and post-hoc linear mixed models (LMMs) on grey matter volume (GMV) in VBM clusters. Depicted are hemisphere, cluster name (derived from CAT12's "neuromorphometrics atlas"), cluster size in voxels, p_{FWE} after threshold-free cluster enhancement (TFCE) correction, coordinates in MNI space (x y z), LMM results, post-hoc-test results, group estimates, and pattern (see Figure 2). The cluster with an extent of 1 voxel was excluded from further analyses. LMM statistical parameters (degrees of freedom (DF), X^2

665 value, p value) were obtained from a full-null model comparison. Post-hoc results include the
666 t-ratio with DF and p value. P<0.05 indicates a significant group-by-time interaction effect.
667 N=63 (stress group=30).

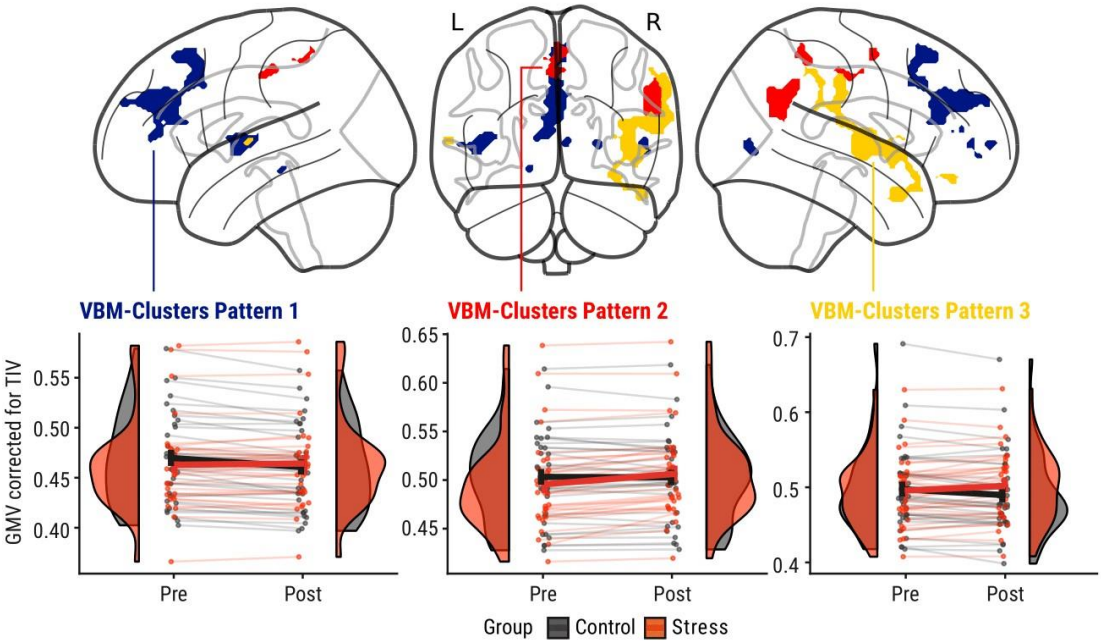

668

669 **Figure 2.** *Top row*: VBM results indicating a significant (p_{FWE}<0.05) group-by-time interaction
670 effect on GMV, colours indicate three distinguishable patterns: pattern 1 (blue) - control:
671 decrease, stress: no significant change; pattern 2 (red) - control: no significant change, stress:
672 increase; pattern 3 (yellow) - control: decrease, stress: increase. *Lower row*: Changes in GMV
673 group distributions (half violin) with individual changes (points, lines) and group means (central
674 line with error bars). N=63 (stress group=30).

675 Analysis of total GM, total WM, and CSF

676 A significant group-by-time interaction effect was found for total GM ($X^2(1)=6.04$,
677 p=0.0140) and CSF ($X^2(1)=4.7$, p=0.0305), while no significant change was found for
678 WM ($X^2(1)=0.20$, p=0.657). Post-hoc tests were not significant for total GM (control:
679 $t/t_c(60.3) = -1.96$, p=0.1084; stress: $t/t_s(62.9) = 1.70$, p=0.1084), but qualitatively
680 showed a decrease in the control group (-0.4%, $\beta_c = -0.004$) and an increase in the
681 stress group (0.4%, $\beta_s = 0.004$). CSF increased significantly in the control group

682 (1.5%, β_c =3.98, t/t$_c$(60.2) = 2.6, p=0.0232) and decreased non-significantly in the
683 stress group (-0.4%, $\beta_s = -1.23$, t/t$_s$(62.3) = -0.7, p=0.4857).

684

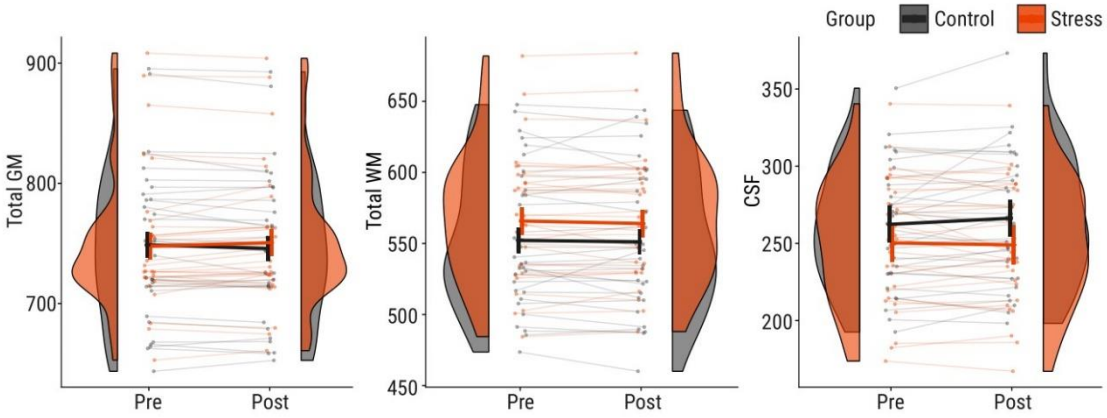

685

686 **Figure 3.** Change in total grey matter (GM), total white matter (WM), and total cerebrospainal
687 fluid (CSF) values in the control group (grey) and in the stress group (red). Shown are scans
688 (points) per subject (thin lines) and group distributions (half violin) for pre- and post-
689 intervention scans. Bold lines indicate estimated marginal means and 95% confidence
690 intervals obtained from linear mixed models. If data were transformed (log$_e$) for statistical
691 analysis, the estimates were back-transformed for visualization. N=63 (stress group=30).

692 # Additional MR parameters in VBM clusters

693 ## T1 values

694 The group-by-time interaction effect found in the VBM data was not significant in the
695 extracted quantitative T1 values (F(1)=0.40, p=0.5297). There was a significant time-
696 by-cluster interaction effect, indicating an increase in T1 values over time (F(14)=9.82,
697 p<0.0001). Post-hoc tests showed this was the case in 7 out of the 15 clusters not
698 including the three biggest clusters in the SMFG and bilateral insula (Table S1, Figure
699 S3). Post-hoc tests and visual inspection of the results (Figure 4) indicated that on
700 average the T1 value increased (~47 ms, ~ 3.4%) with time across groups.

701 A control analysis (see supplement) showed a T1 increase of similar magnitude
702 (29ms, 2.4%, F(1)=40.36, p<0.0001) in GM voxels outside of the VBM-Clusters. To
703 follow-up on this we compared T1values within GM masks produced at different

thresholds (0.1,0.2,0.3). A significant increase in T1 values was found at thresholds of 0.1 (and 0.2 and 0.3), but not at 0.5 (see Table S2), indicating that this effect was driven by the outer edges of GM. We investigated whether the definition of GM boundaries would similarly affect our VBM and found the VBM-results to be robust against those changes.

T1-weighted intensity values

The group-by-time interaction effect found in the VBM data was not significant in the extracted quantitative T1-weighted intensity values ($X^2(1)=3.13$, $p=0.99$). The main effect of time was not significant either ($F(1)= 2.17$, $p=0.141$, Figure 4), but a significant main effect of group ($F(1)= 7.3$, $p= 0.0088$) indicated a difference in initial T1weighted intensity values that remained constant over time.

Cerebral blood flow

For CBF, there was a non-significant trend for a group-by-time interaction across all included clusters ($X^2(1)=3.33$, $p=0.068$). Post-hoc tests in both groups separately showed no significant effect in either group. Qualitatively, CBF decreased in the control group (by 1.1 ml/100mg/min ~2.6%, $t/t_c(951) = -1.82$, $p(cor) = 0.1383$) and increased in the stress group (by 0.4 ml/100mg/min ~1%, $t/t_s(951)= 0.775$, $p=0.4387$), resembling pattern 3 of the VBM results (Figure 4).

In local post-hoc tests, no CBF changes survived multiple-comparison correction (all $p_{corr} > 0.29$). For more details of the CBF results, see supplement.

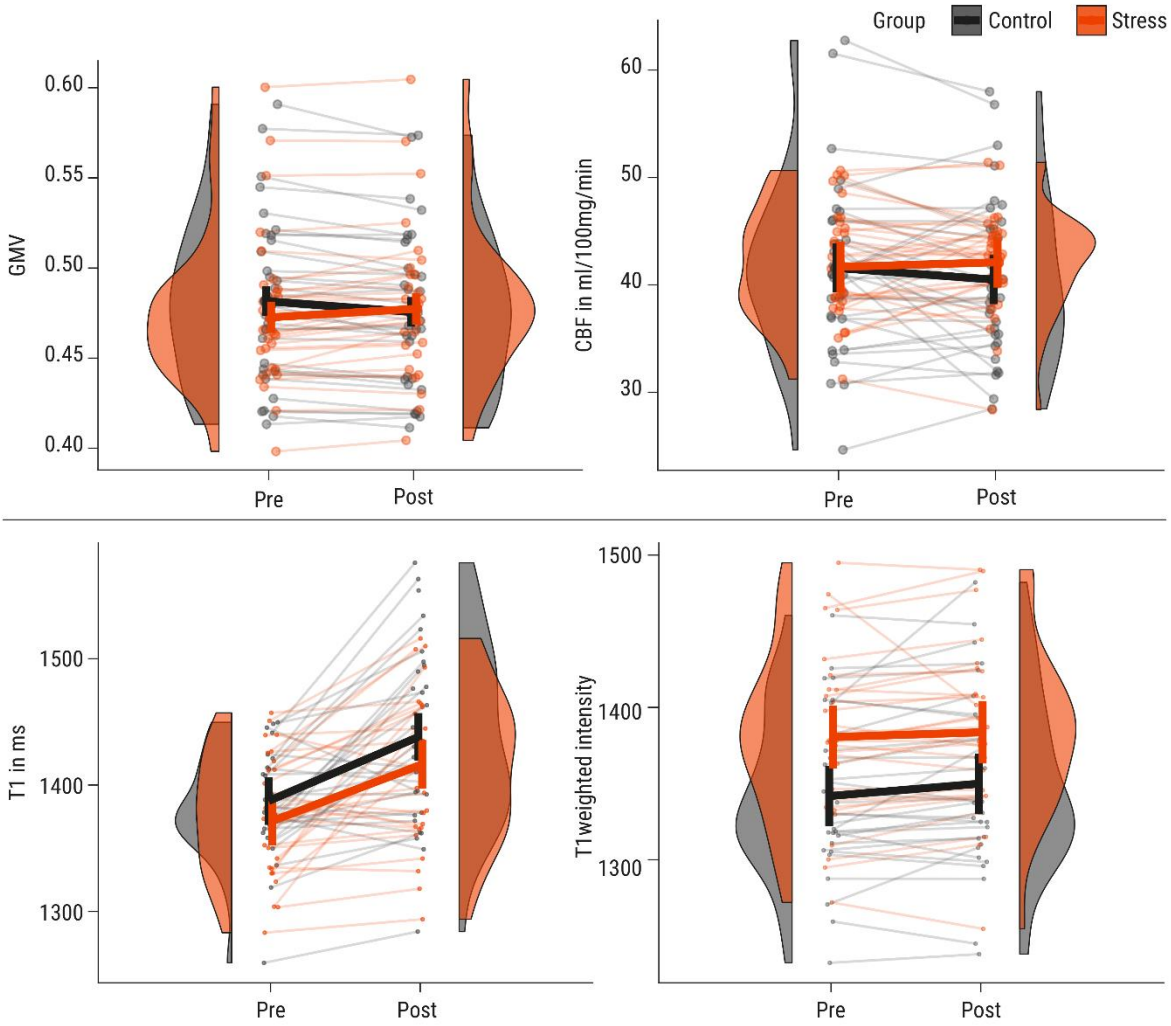

Figure 4: Change in grey matter volume (GMV), cerebral blood flow (CBF), T1, and T1-weighted intensity values in the control group (grey) and in the stress group (red). Shown are scans (points) per subject (thin lines) averaged across clusters and group distributions (half violin) for the pre- and post-intervention scan. Bold lines indicate estimated marginal means and 95% confidence intervals obtained from linear mixed models. If data were transformed ($\log_e$ or square-root) for statistical analysis, the estimates were back-transformed for visualization.

Anatomical ROIs: Amygdala and Hippocampus

Comparing the full to the null model showed no significant group-by-time interaction effect on GMV in the left Amygdala ($X^2(1)=0.60$, $p=0.4372$), right Amygdala ($X^2(1)=0.77$, $p=0.3803$), left Hippocampus ($X^2(1)=0.13$, $p=0.7227$), or right Hippocampus ($X^2(1)=0.02$, $p=0.8805$).

Autonomic, endocrine, and subjective stress measures

The TSST induced a robust stress response in autonomic, endocrine, and subjective stress measures, as also shown in previous publications from our study (Reinelt & Uhlig et al., 2019 and Bae & Reinelt et al., 2019). Significant (p_{corr}<0.05 with Bonferroni-Holm correction) group-by-time interaction effects were present in all investigated autonomic, endocrine, and subjective markers (Table 2 and Figure 5).

Post-hoc tests and visualization (Figure 5) show the dynamics of the stress response: subjective stress peaked earliest (+5 min) and saliva cortisol latest (+25 min). Heart rate was the first parameter to return to baseline (+25 min) while the group difference in saliva cortisol remained longest (+90 min).

Dependent Variable	**N**	**DF**	**X^2**	**p**
Saliva cortisol	64	8	309.1	<0.0001
Plasma ACTH	57	8	216.6	<0.0001
Heart rate	60	12	279.3	<0.0001
Heart rate variability	60	11	44.4	<0.0001
State anxiety (STAI)	66	8	89.7	<0.0001
VAS stressfulness	66	8	71.8	<0.0001

Table 2. Results from linear mixed models on autonomic, endocrine, and subjective stress measures. Statistical parameters were obtained from a full-null-model comparison. Fixed effects: time, group, group-by-time interaction (full model only); Random effects: participant. Depicted are degrees of freedom (DF), the X^2 and the *p* value from the full-null-model comparison. ACTH = adrenocorticotropic hormone; STAI = State Anxiety Inventory.

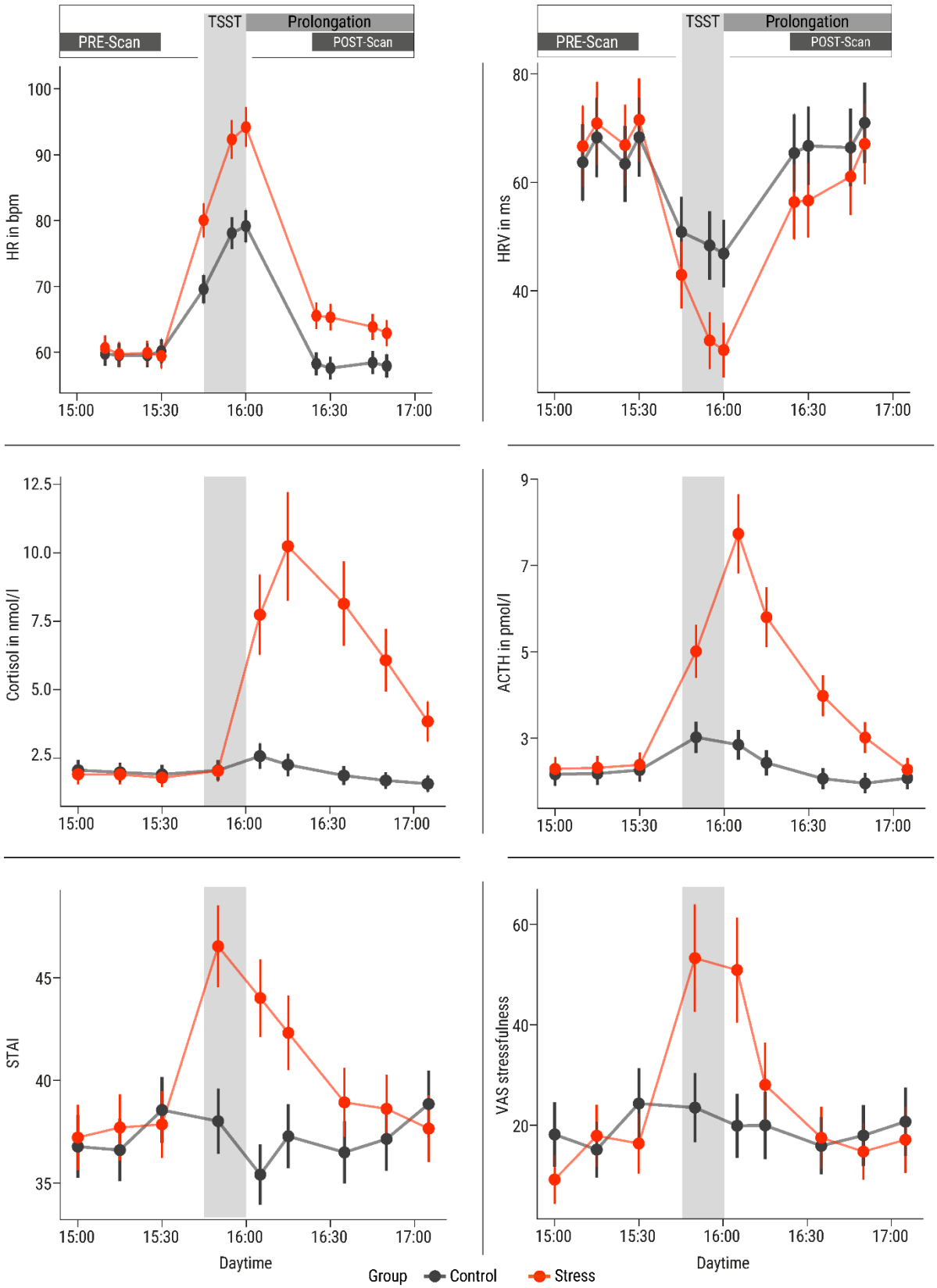

Figure 5: Time courses (x-axis: time of day) of saliva cortisol (nmol/l) and plasma adrenocorticotropic hormone (ACTH) (pmol/l) concentrations, heart rate (beats per minute) and heart rate variability (RMSSD in ms) and subjective stress (sum score) measured by state

anxiety (State Anxiety Inventory, STAI) and a visual analogue scale (VAS) of stressfulness. Plotted are the estimated marginal means from the linear mixed models (see above). If data were transformed ($\log_e$ or square-root) for statistical analysis, the estimates were back-transformed for visualization. Error bars depict upper and lower 95% confidence intervals for model estimates. Grey: control group, orange: stress group. (Only timepoints between the two anatomical scans are included; for the full time courses and their statistical analysis, see Bae & Reinelt, et al., 2019; Reinelt & Uhlig, et al., 2019.)

Association of GMV with other stress measures in VBM clusters

Association of VBM changes with other stress measures

After multiple-comparison correction, no significant association of GMV changes with autonomic (HR and HRV), endocrine (saliva cortisol and plasma ACTH), and subjective (STAI score and VAS-score) stress measures was found in any cluster in the LMM analysis (see Supplement for details).

Association of ΔVBM with peak reactivity of other stress measures

Endocrine stress measures: In the full-null-model comparison, there was no significant effect of saliva cortisol ($F(2)=0.63, p_{corr}=1$) or plasma ACTH peak reactivity ($F(2)=2.03$, $p_{corr}=0.1321$) on ΔGMV (Figure S5).

Autonomic stress measures: In the full-null-model comparison, there was no significant effect of HR peak reactivity ($F(2)=3.51$, $p_{corr}=0.2736$, Figure S5) on ΔGMV. HRV peak reactivity ($F(2)=6.24$, $p_{corr}=0.0224$) was significantly associated with ΔGMV. Post-hoc tests showed no significant interaction effect for group ($t/t(827)= -1.59$, $p=0.1107$), but a negative association between HRV peak reactivity and ΔGMV both in the stress ($\beta_s= -0.0000327$) and the control group ($\beta_c=-0.0000885$).

In both groups, the participants who showed more pronounced HRV decreases also showed stronger GMV increases (or weaker GMV decreases, Figure 6).

Subjective stress measures: In the full-null-model comparison, there was a significant effect of STAI score peak reactivity on ΔGMV ($F(2)=7.586$, $p_{corr}=0.0065$). Post-hoc tests showed a significant interaction effect with group ($t/t(987)=2.335$, $p=0.0197$) and a positive association between STAI score peak reactivity and ΔGMV both in the stress

(β_s=0.0000902) and the control group (β_c=0.0003895). In both groups, the participants who showed more pronounced STAI score increases also showed stronger GMV increases (or weaker GMV decreases, Figure 6).

In the full-null-model comparison, there was no significant effect of VAS stressfulness peak reactivity of ΔGMV ($F(2)=3.879, p_{corr}=0.1894$, Table S6, Figure S5).

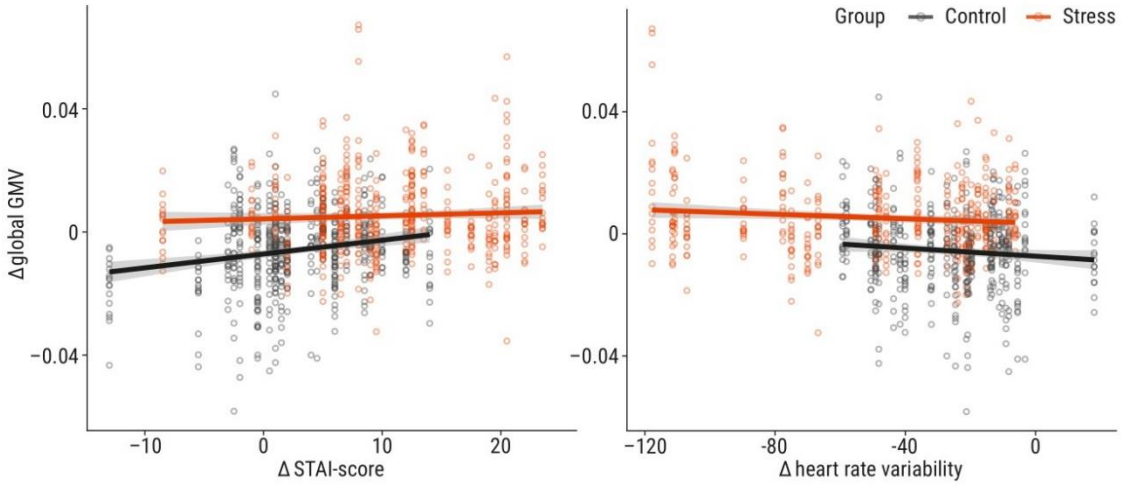

Figure 6: Association of Δ grey matter volume (GMV; post-pre) with peak reactivity of stress measures. Shown are significant associations from linear models (LMs): state anxiety (State Anxiety Inventory, STAI; positive association) and heart rate variability (RMSSD; negative association). The LMs revealed no significant association with saliva cortisol, ACTH, heart rate and subjective stressfulness (Figure S5). Line indicates slope and standard error. Points indicate GMV values per voxel-based morphometry (VBM) cluster and subject, each subject is represented in one column of points. Grey: control group, orange: stress group.

Discussion

Using voxel-based morphometry, we found rapid volumetric brain changes that differed between groups over time in 15 clusters, mainly along the cortical midline and in bilateral insula. We identified three patterns of GMV changes across the clusters: the stress group showed a GMV increase (patterns 2 and 3) or no change (pattern 1) while the control group showed a GMV decrease (patterns 1 and 3) or no change (pattern 2). Our stress intervention induced a pronounced stress response on the autonomic, endocrine, and subjective levels. Changes in GMV were related to peak

reactivity in subjective stress and heart rate variability but not in heart rate, saliva cortisol, plasma ACTH, or subjective stressfulness.

To explore the microstructural and physiological basis of these findings, we also analyzed quantitative T1 and CBF imaging parameters. The significant group difference over time was not present in T1 or T1-weighted intensity values. In T1 values, a significant increase over time across groups occurred, which post-hoc tests showed to be significant in half of the clusters. In addition, no changes in CBF survived multiple-comparison correction, while - qualitatively - CBF changed similarly to pattern 1 of GMV changes (decrease in the control group, no change in the stress group). Thus, the stress-related brain changes are reflected in local GMV increases relative to the control group. In clusters with no significant GMV change, the increase may be masked by the GMV decrease observed in the control group. We did not observe the hypothesized GMV changes in hippocampus and amygdala.

In summary, we found that the dynamics of rapid volumetric brain changes differed between groups, suggesting that endogenous circadian brain changes (GMV decrease) are counteracted by acute stress.

In our study, the two anatomical scans were separated by approximately 2.5 hours, from early to late afternoon. Total GMV has previously been shown to linearly decrease by ~1% from morning to afternoon (Karch et al., 2019). Circadian changes in total GMV can be accompanied by regional GMV changes, for example, in the MPFC and precuneus (Trefler et al., 2016). Thus, the local GMV decrease in the control group may correspond to endogenous circadian changes, which was absent in the stress group. Exogeneous behavioural interventions have been shown to attenuate endogenous daytime effects on GMV (Trefler et al., 2016; Thomas et al., 2016) and so may a stressful intervention like the TSST.

In a follow-up analysis, total GM and CSF changed significantly in the control group (Figure 3): Total GM decreased, while CSF increased from early to late afternoon, following the pattern of circadian rhythm-related GMV changes reported in Trefler et al. (2016). In the stress group, total GM and CSF changed significantly in the opposite direction compared to the control group: GM increased and CSF decreased. Total white matter did not change significantly in both groups. We thus speculate that

processes related to the circadian rhythm (i.e., supporting diurnal brain homeostasis; Trefler et al. 2016) are involved in the changes in our control group, while in the stress group, the behavioural intervention counteracts these processes.

Furthermore, VBM measures of GM have been shown to be affected by hydration status, also suggesting an impact of fluid homeostasis (Streitbürger et al., 2012). While we minimized variability of food and fluid intake by providing a standardized lunch, we cannot exclude the possibility of hydration differences in our study. On the other hand, dehydration mainly affects areas close to the ventricles rather than cingulate and insular cortices (Streitbürger et al., 2012).

In summary, GMV decreases in the control group may reflect circadian changes (e.g., in fluid homeostasis associated with astrocyte swelling or shrinkage). In the stress group, such processes may be counteracted by processes regulating energy demand following neuronal activation in response to the stressful intervention. This increased energy demand following brain activity under stress may also be reflected in increased CBF, which has been shown to affect VBM measures of GMV (Ge et al., 2017).

The rapidness of brain changes we detected with structural MR imaging methods raises the question of their physiological origins. Mouse studies have connected VBM changes to altered dendritic spine density: Aversive, stressful stimulation, like auditory fear conditioning (Keifer et al., 2015) or restraint (Kassem et al., 2013) led to volumetric changes, measured with volumetric MRI (Kassem et al., 2013) or VBM (Keifer et al., 2015), which were correlated with spike density changes in functionally relevant regions, such as amygdala and insula (Keifer et al., 2015) as well as ACC (Kassem et al., 2013). While synaptic and dendritic plasticity may be detectable after minutes to hours, given their size is on the scale of nm to µm, both are unlikely to introduce changes detectable with a 1.5-mm voxel size (Johansen-Berg et al., 2012). Changes to dendritic morphology may rather be accompanied by migration or swelling of capillaries and glia in order to compensate for heightened energy demand resulting in increased tissue volume, which manifests itself as GMV changes detected by VBM (Lövdén et al., 2013). Following the supply-demand model, changes in brain function may thereby precede changes in brain structure (Lövdén et al., 2013).

Astrocytes are prominent candidates for targeting cellular structures in brain plasticity. These non-myelinating glia cells are involved in neuronal metabolism and fluid homeostasis, and they can mediate the excitability of neurons (Shao & McCarthy, 1994). Activation may cause astrocytes to swell within seconds or minutes, leading to a general shift from extra- to intracellular space and affecting MRI measures (Johansen-Berg et al., 2012). Astrocytes also express corticosteroid receptors (Bohn et al., 1991), and their structure and function can be affected by chronic (Tynan et al., 2013) as well as acute stress (Braun et al., 2009). Stress-induced astrocyte plasticity has also been linked to stress-related psychiatric diseases (for a review, see Bender et al., 2016).

Thus, the observed GMV changes may fully or partly reflect (transient) local tissue (e.g., glial) changes and/or vascular changes to accommodate changes in energy demand following neural activity. These alterations, which are present more than an hour after the stress episode, may also be related to the induction of – potentially long-term - morphological changes.

Consistent with the overall GMV decrease in the control group, we find decreased CBF in that group across all clusters (although not statistically significant). In two VBM clusters, we also found CBF increases in the stress group, which, however, also did not survive multiple-comparison correction. Qualitatively, CBF was increased in the left and right SMFG of the stress group, whereas there was no significant effect in the control group. CBF increases have previously been shown (using ASL) during an in-scanner stressor, for example in the right PFC, ACC, insula, and putamen (Wang et al., 2005). Many brain vessels are located along the medial wall, including the middle cerebral artery, but also the insula displays a particularly high density of vessels, including the anterior cerebral artery (Mouches & Forkert, 2019). Thus, our main VBM clusters (bilateral SMFG and insula) are in the vicinity of major vessels. During stress-induced physiological activity, changes in blood parameters (e.g., blood flow) and vasodilation could influence the VBM analysis. Changes in CBF have been shown to closely overlap spatially with changes in VBM (Franklin et al, 2013). However, we did not find significant CBF changes in the two SMFG clusters. One reason may be the limited sensitivity of the pASL analysis due to the relatively low resolution, the time delay to the intervention (~90 min) or limited spatial coverage (Figure S1). On the other

hand, previous studies have shown overlapping but incongruent patterns of CBF and VBM changes (Ge et al., 2017, Franklin et al., 2013), which may indicate that other processes, such as changes in brain metabolites in response to functional activation, may affect the T1-weighted signal and thus contribute to apparent GMV changes measured with VBM (Ge et al., 2017). In line with that, changes in blood oxygenation after a breathing intervention (with an increased CO_2-concentration) affected the estimation of GMV and decreased longitudinal relaxation rate T1 in GM (Tardif et al., 2017). It has been proposed that an intervention-induced increase in oxygen-demand in specific brain areas may similarly affect estimations of GMV through changes in CBF and tissue oxygenation (Tardif et al., 2017). In our study, T1 values showed a significant increase over time in both groups and seven clusters but no significant group difference, that is, the VBM interaction was not mirrored in T1 values. This increase in T1 values was not limited to the VBM clusters but occurred in all GM. With an increasing threshold of GM definition (probability of this voxel being in GM), the magnitude of this main effect of time decreased (0.1: 29 ms, 0.2: 24 ms, 0.3: 20 ms) and was not significant at a threshold of 0.5 (2 ms). This indicates that the T1 increase was stronger near the tissue boundaries of GM and CSF. Likewise, VBM clusters with a significant increase in T1 were often located in frontal and parietal areas (Figure S3). Since T1 is strongly related to water content of tissue (Mathur-De Vré 1984), this could suggest an inflow of CSF, which was supported by a significant increase in total CSF volume in the control group, but not in the stress group. The T1-weighted intensity values did not show any significant changes.

Functionally, the main clusters of stress related VBM changes in cortical midline structures (CMS) and bilateral insula can be related to the processing of emotional/stressful and self-relevant information.

The biggest cluster extended from the superior medial frontal cortex to the anterior cingulate cortex. Functionally, the medial frontal cortex has been involved in emotion processing (Etkin et al., 2011) and in the regulation of the physiological and behavioural stress response (McKlveen et al., 2015). It also has a high density of glucocorticoid receptors, which are central to the negative feedback mechanism of the HPA axis (Buchanan et al., 2010). Yet, we found no significant association of GMV with endocrine stress measures.

A significant association was found with the subjective and autonomic stress measures of state anxiety (STAI) and HRV, respectively. Decreased HRV correlated inversely with GMV changes in both groups, suggesting that control participants whose parasympathetic activity changed similarly to participants in the stress group showed less decrease in GMV than other control participants. In parallel, higher state anxiety was associated with less GMV decrease in both groups, but even stronger in the control group. These results indicate that parasympathetic deactivation and state anxiety, which can result from psychological stress, are linearly associated with GMV changes, and counteract the GMV decrease. In general, CMS – especially anterior ones – have been associated with self-relatedness and self-relevance (for a review, see Northoff & Bermpohl, 2004), a feature of any stressor and particularly of the TSST, in which participants "apply" for their individual dream jobs. Although participants knew the job interview was not real, they showed pronounced stress responses. Negative self-relevant stimuli and psychosocial stress have been shown to increase activity in CMS (e.g., MPFC; Lemogne et al., 2011) as well as connectivity between the amygdala and CMS (Veer et al., 2011), respectively.

In our study, two major clusters of stress related GMV changes showed peaks in the left anterior insula and the right posterior insula. The insula has been understood as primary viscerosensory or interoceptive cortex with a posterior-to-anterior gradient (Craig, 2002): pain, temperature, and other homeostatically relevant bodily stimuli enter the posterior insula before they are integrated with other (e.g., exteroceptive) information and evaluated in the anterior insula, influencing subjective experience and guiding behavior (Craig, 2002). The insula is also highly connected and often co-active with frontal CMS (e.g., MPFC and ACC), where the strongest cluster of stress-related GMV changes was found in our study, and they constitute a central axis of the salience network, which processes homeostatically relevant stimuli (Seeley, 2019). The integrative, multisensory function of the insula is also supported by animal studies showing, for example, that the posterior insula can shift behavioural strategies upon the detection of aversive or stressful interoceptive states (Gehrlach et al., 2019).

While we did not investigate functional activation in the current analysis, we have previously shown increased connectivity to the thalamus in response to stress (Reinelt & Uhlig et al., 2019) and it is likely that increased brain activity and/or CBF in relevant areas follow our stress intervention. Indeed, we find a (non-significant) increase from

pre- to post- intervention in CBF in the bilateral SMFG of the stress but not the control group.

In contrast to our hypothesis, we did not find significant GMV changes in hippocampus and amygdala. In animal models of acute stress (Kassem et al., 2013, Chakraborty et al. 2020) and in stress-related mental disorders in humans (Chen et al., 2006; Karl et al., 2006) stress-induced brain changes in hippocampus and amygdala are found. At sub-clinical levels of chronic stress however, some studies did find changes in GMV (Dedovic et al., 2010; Savic, 2015; Suffren et al., 2021; Spalletta et al., 2014, but others did not: GMV reductions associated with stressful life events were, for example, found in the ACC, hippocampus, and parahippocampal gyrus, but not in the amygdala (Papagni et al., 2011) as well as in the MPFC and right insula, but not in the hippocampus or amygdala (Ansell et al., 2012). Possibly, GMV alterations in hippocampus and amygdala may be related to pathophysiological processes in the context of chronic or severe stress (Ansell et al., 2012) rather than the brain response to acute stress.

Limitations

There are several limitations to our study. VBM (and MRI in general) can be considered a physiologically coarse method, and, despite several candidate processes (discussed above), the physiological origin of GMV (MRI) changes remains unclear. VBM has also been criticized for introducing bias and neglecting non-linear effects, which are more pronounced when comparing heterogeneous groups (Bookstein, 2001; Davatzikos, 2004). By comparing two (randomly assigned) groups from a homogenous sample in our study, we expected to minimize potential biases. The inclusion of young, healthy, male participants allowed us to investigate stress-induced changes using a multimodal approach without confounds like the impact of the ovarian cycle. However, the generalisability of our results remains to be tested in studies with more heterogeneous samples. The significant group-by-time interaction effect on GMV suggests that the differences are intervention-induced. While we kept the procedure as similar as possible between groups, we extended the TSST stressor by telling participants in the stress but not the control group there would be another task. Thus, it is possible that not the TSST alone but the prolongation of the stressor (or stress-related vigilance) in the stress group accounts for the group difference in

GMV. Furthermore, a higher temporal resolution would add information about the trajectory of changes and about possible immediate transient changes and the stability of changes we observed in the stress and in the control group. Head motion is a major neuroimaging confound (Beyer et al., 2020.), and it can decrease measures of GMV (Reuter et al., 2015). We aimed to physically minimize head motion during data acquisition and included the realignment / motion parameter MFD from the preceding resting-state scans as a proxy covariate in the VBM analyses. Head motion parameters (e.g., using gyrometry or video-based measures) from the actual MP2RAGE scan could be acquired using additional hardware.

Conclusion

We find rapid differential brain changes following a psychosocial stress intervention versus a placebo version of that task. Brain changes are observed in areas associated with the processing of emotional and self-relevant information, but also with regulating HPA axis activity and sympathetic arousal. Stressed participants additionally show (non-significantly) increased cerebral blood flow in prefrontal areas. Neither changes in CBF nor in T1 or T1-weighted intensity values account for the observed group differences over time. Our findings of rapid GMV changes following acute psychosocial stress detected with MRI in humans emphasize the influence of stress on the brain, suggesting that diurnal mechanisms of brain homeostasis are perturbed by acute stress.

Acknowledgements

The visualization functions for LMM diagnostics were kindly provided by Dr. Roger Mundry.

Conflict of Interest

We have no conflicts of interest to declare.

Data availability

The data that support the findings of this study are openly available in https://osf.io/vjyan/?view_only=c5873b39b3234453a625575192361057. In agreement with participant consent, this includes only derived data, which cannot be used to identify individual participants. The code to reproduce the analysis can be found on https://gitlab.gwdg.de/necos/vbm.git.

References

Allen, M., Poggiali, D., Whitaker, K., Marshall, T. R., & Kievit, R. A. (2019). Raincloud plots: a multi-platform tool for robust data visualization. *Wellcome Open Research*, *4*, 63. https://doi.org/10.12688/wellcomeopenres.15191.1

Ansell, E. B., Rando, K., Tuit, K., Guarnaccia, J., & Sinha, R. (2012). Cumulative Adversity and Smaller Gray Matter Volume in Medial Prefrontal, Anterior Cingulate, and Insula Regions. In *Biological Psychiatry*, 72(1), 57–64. https://doi.org/10.1016/j.biopsych.2011.11.022

Ashburner, J., & Friston, K. J. (2000). Voxel-based morphometry--the methods. *NeuroImage*, *11*(6 Pt 1), 805–821. https://doi.org/10.1006/nimg.2000.0582

Babayan, A., Erbey, M., Kumral, D., Reinelt, J. D., Reiter, A. M. F., Röbbig, J., Lina Schaare, H., Uhlig, M., Anwander, A., Bazin, P.-L., Horstmann, A., Lampe, L., Nikulin, V. V., Okon-Singer, H., Preusser, S., Pampel, A., Rohr, C. S., Sacher, J., Thöne-Otto, A., … Villringer, A. (2019). A mind-brain-body dataset of MRI, EEG, cognition, emotion, and peripheral physiology in young and old adults. *Scientific Data,* 6(1). https://doi.org/10.1038/sdata.2018.308

Bae, Y. J., Reinelt, J., Netto, J., Uhlig, M., Willenberg, A., Ceglarek, U., Villringer, A., Thiery, J., Gaebler, M., & Kratzsch, J. (2019). Salivary cortisone, as a biomarker for psychosocial stress, is associated with state anxiety and heart rate. *Psychoneuroendocrinology*, *101*, 35–41. https://doi.org/10.1016/j.psyneuen.2018.10.015

Barth, C., Steele, C. J., Mueller, K., Rekkas, V. P., Arélin, K., Pampel, A., Burmann, I., Kratzsch, J., Villringer, A., & Sacher, J. (2016). In-vivo Dynamics of the Human Hippocampus across the Menstrual Cycle. *Scientific Reports*, *6*, 32833. https://doi.org/10.1038/srep32833

Bates, D., Mächler, M., Bolker, B., & Walker, S. (2015). Fitting Linear Mixed-Effects Models Usinglme4. *Journal of Statistical Software,* 67(1). https://doi.org/10.18637/jss.v067.i01

Bender, C. L., Calfa, G. D., & Molina, V. A. (2016). Astrocyte plasticity induced by emotional stress: A new partner in psychiatric physiopathology? *Progress in*

Neuro-Psychopharmacology & Biological Psychiatry, *65*, 68–77. https://doi.org/10.1016/j.pnpbp.2015.08.005

Beyer, F., Prehn, K., Wüsten, K. A., Villringer, A., Ordemann, J., Flöel, A., & Witte, A. V. (2020). Weight loss reduces head motion: re-visiting a major confound in neuroimaging. *Human Brain Mapping, 41(9). 2490-2494*, https://doi.org/10.1101/766261

Bohn, M. C., Howard, E., Vielkind, U., & Krozowski, Z. (1991). Glial cells express both mineralocorticoid and glucocorticoid receptors. *The Journal of Steroid Biochemistry and Molecular Biology*, *40*(1-3), 105–111. https://doi.org/10.1016/0960-0760(91)90173-3

Bookstein, F. L. (2001). “Voxel-based morphometry” should not be used with imperfectly registered images. *NeuroImage*, *14*(6), 1454–1462. https://doi.org/10.1006/nimg.2001.0770

Braun, K., Antemano, R., Helmeke, C., Büchner, M., & Poeggel, G. (2009). Juvenile separation stress induces rapid region- and layer-specific changes in S100ss- and glial fibrillary acidic protein-immunoreactivity in astrocytes of the rodent medial prefrontal cortex. *Neuroscience*, *160*(3), 629–638. https://doi.org/10.1016/j.neuroscience.2009.02.074

Buchanan, T. W., Driscoll, D., Mowrer, S. M., Sollers, J. J., 3rd, Thayer, J. F., Kirschbaum, C., & Tranel, D. (2010). Medial prefrontal cortex damage affects physiological and psychological stress responses differently in men and women. *Psychoneuroendocrinology*, *35*(1), 56–66. https://doi.org/10.1016/j.psyneuen.2009.09.006

Chakraborty, P., Datta, S., McEwen, Bruce S., Chattarji, S. (2020) Corticosterone after Acute Stress Prevents the Delayed Effects on the Amygdala. Neuropsychopharmacology, 45(13), 2139–46. https://doi.org/10.1038/s41386-020-0758-0.

Chen, S., Xia, W., Li, L., Liu, J., He, Z., Zhang, Z., Yan, L., Zhang, J., & Hu, D. (2006). Gray matter density reduction in the insula in fire survivors with posttraumatic stress disorder: a voxel-based morphometric study. *Psychiatry Research*, *146*(1), 65–72. https://doi.org/10.1016/j.pscychresns.2005.09.006

Chen, Y., Rex, C. S., Rice, C. J., Dubé, C. M., Gall, C. M., Lynch, G., & Baram, T. Z. (2010). Correlated memory defects and hippocampal dendritic spine loss after acute stress involve corticotropin-releasing hormone signaling. Proceedings of the National Academy of Sciences, 107(29), 13123–13128. https://doi.org/10.1073/pnas.1003825107

Chrousos, G. P. (2009). Stress and disorders of the stress system. *Nature Reviews Endocrinology*, 5 (7), 374–381. https://doi.org/10.1038/nrendo.2009.106

Cohen, S., Tyrrell, D. A., & Smith, A. P. (1991). Psychological stress and susceptibility to the common cold. *The New England Journal of Medicine*, *325*(9), 606–612. https://doi.org/10.1056/NEJM199108293250903

Craig, A. D. (2002). How do you feel? Interoception: the sense of the physiological condition of the body. *Nature Reviews. Neuroscience*, *3*(8), 655–666. https://doi.org/10.1038/nrn894

Czéh, B., Simon, M., Schmelting, B., Hiemke, C., & Fuchs, E. (2006). Astroglial plasticity in the hippocampus is affected by chronic psychosocial stress and concomitant fluoxetine treatment. *Neuropsychopharmacology: Official Publication of the American College of Neuropsychopharmacology*, *31*(8), 1616–1626. https://doi.org/10.1038/sj.npp.1300982

Davatzikos, C. (2004). Why voxel-based morphometric analysis should be used with great caution when characterizing group differences. *NeuroImage*, *23*(1), 17–20. https://doi.org/10.1016/j.neuroimage.2004.05.010

Dedovic, K., Engert, V., Duchesne, A., Lue, S. D., Andrews, J., Efanov, S. I., Beaudry, T., & Pruessner, J. C. (2010). Cortisol awakening response and hippocampal volume: vulnerability for major depressive disorder? *Biological Psychiatry*, *68*(9), 847–853. https://doi.org/10.1016/j.biopsych.2010.07.025

Dedovic, K., Rexroth, M., Wolff, E., Duchesne, A., Scherling, C., Beaudry, T., Lue, S. D., Lord, C., Engert, V., & Pruessner, J. C. (2009). Neural correlates of processing stressful information: an event-related fMRI study. *Brain Research*, *1293*, 49–60. https://doi.org/10.1016/j.brainres.2009.06.044

Draganski B, Gaser C, Busch V, Schuierer G, Bogdahn U, May A. (2004) Neuroplasticity: changes in grey matter induced by training. *Nature*, 427, 311–312. https://doi.org/10.1038/427311a

Eickhoff, S. B., Stephan, K. E., Mohlberg, H., Grefkes, C., Fink, G. R., Amunts, K., & Zilles, K. (2005). A new SPM toolbox for combining probabilistic cytoarchitectonic maps and functional imaging data. *NeuroImage*, *25*(4), 1325–1335. https://doi.org/10.1016/j.neuroimage.2004.12.034

Engert, V., Efanov, S. I., Duchesne, A., Vogel, S., Corbo, V., & Pruessner, J. C. (2013). Differentiating anticipatory from reactive cortisol responses to psychosocial stress. *Psychoneuroendocrinology*, *38*(8), 1328–1337. https://doi.org/10.1016/j.psyneuen.2012.11.018

Etkin, A., Egner, T., & Kalisch, R. (2011). Emotional processing in anterior cingulate and medial prefrontal cortex. *Trends in Cognitive Sciences*, *15*(2), 85–93. https://doi.org/10.1016/j.tics.2010.11.004

Forstmeier, W., & Schielzeth, H. (2011). Cryptic multiple hypotheses testing in linear models: overestimated effect sizes and the winner's curse. *Behavioral Ecology and Sociobiology*, *65*(1), 47–55. https://doi.org/10.1007/s00265-010-1038-5

Fox, J., & Weisberg, S. (2018). *An R Companion to Applied Regression*. SAGE Publications. https://play.google.com/store/books/details?id=SfNrDwAAQBAJ

Franklin, T. R., Wang, Z., Shin, J., Jagannathan, K., Suh, J. J., Detre, J. A., O'Brien, C. P., & Childress, A. R. (2013). A VBM study demonstrating "apparent" effects of a single dose of medication on T1-weighted MRIs. *Brain Structure & Function*, *218*(1), 97–104. https://doi.org/10.1007/s00429-012-0385-6

Gaudl, A., Kratzsch, J., Bae, Y. J., Kiess, W., Thiery, J., & Ceglarek, U. (2016). Liquid chromatography quadrupole linear ion trap mass spectrometry for quantitative steroid hormone analysis in plasma, urine, saliva and hair. *Journal of Chromatography. A*, *1464*, 64–71. https://doi.org/10.1016/j.chroma.2016.07.087

Gehrlach, D. A., Dolensek, N., Klein, A. S., Chowdhury, R. R., Matthys, A., Junghänel, M., Gaitanos, T. N., Podgornik, A., Black, T. D., Vaka, N. R., Conzelmann, K.-K., & Gogolla, N. (2019). Aversive state processing in the

1158 posterior insular cortex. *Nature Neuroscience,* 22(9), 1424–1437.
1159 https://doi.org/10.1038/s41593-019-0469-1

1160 Ge, Q., Peng, W., Zhang, J., Weng, X., Zhang, Y., Liu, T., Zang, Y.-F., & Wang, Z.
1161 (2017). Short-term apparent brain tissue changes are contributed by cerebral
1162 blood flow alterations. *PloS One*, *12*(8), e0182182.
1163 https://doi.org/10.1371/journal.pone.0182182

1164 Gould, E., Tanapat, P., McEwen, B. S., Flügge, G., & Fuchs, E. (1998). Proliferation
1165 of granule cell precursors in the dentate gyrus of adult monkeys is diminished
1166 by stress. *Proceedings of the National Academy of Sciences of the United*
1167 *States of America*, *95*(6), 3168–3171. https://doi.org/10.1073/pnas.95.6.3168

1168 Haddock B, Larsson HB, Hansen AE, Rostrup E. (2013) Measurement of brain
1169 oxygenation changes using dynamic T1-weighted imaging. *Neuroimage*, 78:7-
1170 15. https://doi.org/10.1016/j.neuroimage.2013.03.068

1171 Heine, V. M., Maslam, S., Zareno, J., Joëls, M., & Lucassen, P. J. (2004).
1172 Suppressed proliferation and apoptotic changes in the rat dentate gyrus after
1173 acute and chronic stress are reversible. *The European Journal of Neuroscience*,
1174 *19*(1), 131–144. https://doi.org/10.1046/j.1460-9568.2003.03100.x

1175 Herman, J. P., Figueiredo, H., Mueller, N. K., Ulrich-Lai, Y., Ostrander, M. M., Choi,
1176 D. C., & Cullinan, W. E. (2003). Central mechanisms of stress integration:
1177 hierarchical circuitry controlling hypothalamo–pituitary–adrenocortical
1178 responsiveness. *Frontiers in Neuroendocrinology*, 24(3), 151–180).
1179 https://doi.org/10.1016/j.yfrne.2003.07.001

1180 Hermans, E. J., Henckens, M. J. A. G., Joëls, M., & Fernández, G. (2014). Dynamic
1181 adaptation of large-scale brain networks in response to acute stressors. *Trends*
1182 *in Neurosciences*, *37*(6), 304–314. https://doi.org/10.1016/j.tins.2014.03.006

1183 Het, S., Rohleder, N., Schoofs, D., Kirschbaum, C., & Wolf, O. T. (2009).
1184 Neuroendocrine and psychometric evaluation of a placebo version of the “Trier
1185 Social Stress Test.” In *Psychoneuroendocrinology*, 34(7), 1075–1086.
1186 https://doi.org/10.1016/j.psyneuen.2009.02.008

1187 He, Y., Chen, Z. J., & Evans, A. C. (2007). Small-world anatomical networks in the
1188 human brain revealed by cortical thickness from MRI. *Cerebral Cortex* , *17*(10),

2407–2419. https://doi.org/10.1093/cercor/bhl149

Höflich, A., Ganger, S., Tik, M., Hahn, A., Kranz, G. S., Vanicek, T., Spies, M., Kraus, C., Windischberger, C., Kasper, S., Winkler, D., & Lanzenberger, R. (2017). Imaging the neuroplastic effects of ketamine with VBM and the necessity of placebo control. In *NeuroImage,* 147, 198–203). https://doi.org/10.1016/j.neuroimage.2016.12.032

Holm, S. (1979). A simple sequentially rejective multiple test procedure. Scandinavian Journal of Statistics, *6*, 65–70. https://www.jstor.org/stable/4615733.

Jenkinson, M., Beckmann, C. F., Behrens, T. E. J., Woolrich, M. W., & Smith, S. M. (2012). FSL. *NeuroImage*, *62*(2), 782–790. https://doi.org/10.1016/j.neuroimage.2011.09.015

Joëls, M., Pasricha, N., & Karst, H. (2013). The interplay between rapid and slow corticosteroid actions in brain. *European Journal of Pharmacology*, *719*(1-3), 44–52. https://doi.org/10.1016/j.ejphar.2013.07.015

Johansen-Berg, H., Baptista, C. S., & Thomas, A. G. (2012). Human structural plasticity at record speed [Review of *Human structural plasticity at record speed*]. *Neuron*, *73*(6), 1058–1060. https://doi.org/10.1016/j.neuron.2012.03.001

Karch, J. D., Filevich, E., Wenger, E., Lisofsky, N., Becker, M., Butler, O., Mårtensson, J., Lindenberger, U., Brandmaier, A. M., & Kühn, S. (2019). Identifying predictors of within-person variance in MRI-based brain volume estimates. *NeuroImage*, *200*, 575–589. https://doi.org/10.1016/j.neuroimage.2019.05.030

Karl, A., Schaefer, M., Malta, L. S., Dörfel, D., Rohleder, N., & Werner, A. (2006). A meta-analysis of structural brain abnormalities in PTSD. *Neuroscience and Biobehavioral Reviews*, *30*(7), 1004–1031. https://doi.org/10.1016/j.neubiorev.2006.03.004

Kassem, M. S., Lagopoulos, J., Stait-Gardner, T., Price, W. S., Chohan, T. W., Arnold, J. C., Hatton, S. N., & Bennett, M. R. (2013). Stress-induced grey matter loss determined by MRI is primarily due to loss of dendrites and their synapses.

Molecular Neurobiology, *47*(2), 645–661. https://doi.org/10.1007/s12035-012-8365-7

Keifer, O. P., Jr, Hurt, R. C., Gutman, D. A., Keilholz, S. D., Gourley, S. L., & Ressler, K. J. (2015). Voxel-based morphometry predicts shifts in dendritic spine density and morphology with auditory fear conditioning. *Nature Communications*, *6*, 7582. https://doi.org/10.1038/ncomms8582

Kemeny, M. E. (2003). The Psychobiology of Stress. In *Current Directions in Psychological Science,* 12 (4), 124–129. https://doi.org/10.1111/1467-8721.01246

Kirschbaum, C., Pirke, K. M., & Hellhammer, D. H. (1993). The "Trier Social Stress Test"--a tool for investigating psychobiological stress responses in a laboratory setting. *Neuropsychobiology*, *28*(1-2), 76–81. https://doi.org/10.1159/000119004

Lanius, R. A., Williamson, P. C., Bluhm, R. L., Densmore, M., Boksman, K., Neufeld, R. W. J., Gati, J. S., & Menon, R. S. (2005). Functional connectivity of dissociative responses in posttraumatic stress disorder: a functional magnetic resonance imaging investigation. *Biological Psychiatry*, *57*(8), 873–884. https://doi.org/10.1016/j.biopsych.2005.01.011

Laux, L. (1981). *Das State-Trait-Angstinventar: theoret. Grundlagen u. Handanweisung*. https://books.google.com/books/about/Das_State_Trait_Angstinventar.html?hl=&id=-sO6cQAACAAJ

Laux, L., & Spielberger, C. D. (2001). *Das State-Trait-Angstinventar: STAI*. https://books.google.com/books/about/Das_State_Trait_Angstinventar.html?hl=&id=m1VTcgAACAAJ

Lemogne, C., Gorwood, P., Bergouignan, L., Pélissolo, A., Lehéricy, S., & Fossati, P. (2011). Negative affectivity, self-referential processing and the cortical midline structures. In *Social Cognitive and Affective Neuroscience,* 6 (4), 426–433. https://doi.org/10.1093/scan/nsq049

Lisofsky, N., Mårtensson, J., Eckert, A., Lindenberger, U., Gallinat, J., & Kühn, S. (2015). Hippocampal volume and functional connectivity changes during the female menstrual cycle. *NeuroImage*, *118*, 154–162.

https://doi.org/10.1016/j.neuroimage.2015.06.012

Lotze, M., Domin, M., Schmidt, C. O., Hosten, N., Grabe, H. J., & Neumann, N. (2020). Income is associated with hippocampal/amygdala and education with cingulate cortex grey matter volume. *Scientific Reports*, *10*(1), 18786. https://doi.org/10.1038/s41598-020-75809-9

Lövdén, M., Bäckman, L., Lindenberger, U., Schaefer, S., & Schmiedek, F. (2010). A theoretical framework for the study of adult cognitive plasticity. *Psychological Bulletin,* 136 (4), 659–676. https://doi.org/10.1037/a0020080

Lövdén, M., Wenger, E., Mårtensson, J., Lindenberger, U., & Bäckman, L. (2013). Structural brain plasticity in adult learning and development. *Neuroscience and Biobehavioral Reviews*, *37*(9 Pt B), 2296–2310. https://doi.org/10.1016/j.neubiorev.2013.02.014

Malik, M., Bigger, J. T., Camm, A. J., Kleiger, R. E., Malliani, A., Moss, A. J., & Schwartz, P. J. (1996). Heart rate variability: Standards of measurement, physiological interpretation, and clinical use. In *European Heart Journal,* 17 (3), 354–381. https://doi.org/10.1093/oxfordjournals.eurheartj.a014868

Marques, J. P., Kober, T., Krueger, G., van der Zwaag, W., Van de Moortele, P.-F., & Gruetter, R. (2010). MP2RAGE, a self bias-field corrected sequence for improved segmentation and T1-mapping at high field. *NeuroImage*, *49*(2), 1271–1281. https://doi.org/10.1016/j.neuroimage.2009.10.002

Mathôt, S., Schreij, D., & Theeuwes, J. (2012). OpenSesame: an open-source, graphical experiment builder for the social sciences. *Behavior Research Methods*, *44*(2), 314–324. https://doi.org/10.3758/s13428-011-0168-7

Mathur-De Vré, R. (1984). Biomedical implications of the relaxation behaviour of water related to NMR imaging. The British Journal of Radiology, 57(683), 955–976. https://doi.org/10.1259/0007-1285-57-683-955

McEwen, B. S. (2005). Glucocorticoids, depression, and mood disorders: structural remodeling in the brain. *Metabolism: Clinical and Experimental*, *54*(5 Suppl 1), 20–23. https://doi.org/10.1016/j.metabol.2005.01.008

McEwen, B. S., & Gianaros, P. J. (2010). Central role of the brain in stress and adaptation: links to socioeconomic status, health, and disease. *Annals of the*

New York Academy of Sciences, *1186*, 190–222. https://doi.org/10.1111/j.1749-6632.2009.05331.x

McEwen, B. S., & Gianaros, P. J. (2011). Stress- and allostasis-induced brain plasticity. *Annual Review of Medicine*, *62*, 431–445. https://doi.org/10.1146/annurev-med-052209-100430

McKlveen, J. M., Myers, B., & Herman, J. P. (2015). The medial prefrontal cortex: coordinator of autonomic, neuroendocrine and behavioural responses to stress. *Journal of Neuroendocrinology*, *27*(6), 446–456. https://doi.org/10.1111/jne.12272

Miller, R., Plessow, F., Kirschbaum, C., & Stalder, T. (2013). Classification criteria for distinguishing cortisol responders from nonresponders to psychosocial stress: evaluation of salivary cortisol pulse detection in panel designs. *Psychosomatic Medicine*, *75*(9), 832–840. https://doi.org/10.1097/PSY.0000000000000002

Mouches, P., & Forkert, N. D. (2019). A statistical atlas of cerebral arteries generated using multi-center MRA datasets from healthy subjects. *Scientific Data*, *6*(1), 29. https://doi.org/10.1038/s41597-019-0034-5

Nader, N., Chrousos, G. P., & Kino, T. (2010). Interactions of the circadian CLOCK system and the HPA axis. *Trends in Endocrinology and Metabolism: TEM*, *21*(5), 277–286. https://doi.org/10.1016/j.tem.2009.12.011

Nakamura, K., Brown, R. A., Narayanan, S., Collins, D. L., Arnold, D. L., & Alzheimer's Disease Neuroimaging Initiative. (2015). Diurnal fluctuations in brain volume: Statistical analyses of MRI from large populations. *NeuroImage*, *118*, 126–132. https://doi.org/10.1016/j.neuroimage.2015.05.077

Nesse, R. M., Bhatnagar, S., & Ellis, B. (2016). Evolutionary Origins and Functions of the Stress Response System. In *Stress: Concepts, Cognition, Emotion, and Behavior* (pp. 95–101). https://doi.org/10.1016/b978-0-12-800951-2.00011-x

Nicolaides, N. C., Charmandari, E., Chrousos, G. P., & Kino, T. (2014). Circadian endocrine rhythms: the hypothalamic-pituitary-adrenal axis and its actions. *Annals of the New York Academy of Sciences*, *1318*, 71–80. https://doi.org/10.1111/nyas.12464

Nierhaus, T., Vidaurre, C., Sannelli, C., Mueller, K.-R., & Villringer, A. (2021).

1313 Immediate brain plasticity after one hour of brain-computer interface (BCI). *The*
1314 *Journal of Physiology*, *599*(9), 2435–2451. https://doi.org/10.1113/JP278118

1315 Northoff, G., & Bermpohl, F. (2004). Cortical midline structures and the self. *Trends*
1316 *in Cognitive Sciences*, *8*(3), 102–107. https://doi.org/10.1016/j.tics.2004.01.004

1317 Orban, C., Kong, R., Li, J., Chee, M. W. L., & Yeo, B. T. T. (2020). Time of day is
1318 associated with paradoxical reductions in global signal fluctuation and functional
1319 connectivity. *PLoS Biology*, *18*(2), e3000602.
1320 https://doi.org/10.1371/journal.pbio.3000602

1321 Papagni, S. A., Benetti, S., Arulanantham, S., McCrory, E., McGuire, P., & Mechelli,
1322 A. (2011). Effects of stressful life events on human brain structure: a longitudinal
1323 voxel-based morphometry study. *Stress* , *14*(2), 227–232.
1324 https://doi.org/10.3109/10253890.2010.522279

1325 Power, J. D., Schlaggar, B. L., & Petersen, S. E. (2015). Recent progress and
1326 outstanding issues in motion correction in resting state fMRI. *NeuroImage*, *105*,
1327 536–551. https://doi.org/10.1016/j.neuroimage.2014.10.044

1328 Pruessner, J. C., Dedovic, K., Khalili-Mahani, N., Engert, V., Pruessner, M., Buss,
1329 C., Renwick, R., Dagher, A., Meaney, M. J., & Lupien, S. (2008). Deactivation of
1330 the limbic system during acute psychosocial stress: evidence from positron
1331 emission tomography and functional magnetic resonance imaging studies.
1332 *Biological Psychiatry*, *63*(2), 234–240.
1333 https://doi.org/10.1016/j.biopsych.2007.04.041

1334 Radley, J., Morilak, D., Viau, V., & Campeau, S. (2015). Chronic stress and brain
1335 plasticity: Mechanisms underlying adaptive and maladaptive changes and
1336 implications for stress-related CNS disorders. *Neuroscience and Biobehavioral*
1337 *Reviews*, *58*, 79–91. https://doi.org/10.1016/j.neubiorev.2015.06.018

1338 Reinelt, J., Uhlig, M., Müller, K., Lauckner, M. E., Kumral, D., Schaare, H. L.,
1339 Baczkowski, B. M., Babayan, A., Erbey, M., Roebbig, J., Reiter, A., Bae, Y.-J.,
1340 Kratzsch, J., Thiery, J., Hendler, T., Villringer, A., & Gaebler, M. (2019). Acute
1341 psychosocial stress alters thalamic network centrality. *NeuroImage*, *199*, 680–
1342 690. https://doi.org/10.1016/j.neuroimage.2019.06.005

1343 Reuter, M., Tisdall, M. D., Qureshi, A., Buckner, R. L., van der Kouwe, A. J. W., &

1344 Fischl, B. (2015). Head motion during MRI acquisition reduces gray matter
1345 volume and thickness estimates. *NeuroImage*, *107*, 107–115.
1346 https://doi.org/10.1016/j.neuroimage.2014.12.006

1347 Rogers, M. A., Yamasue, H., Abe, O., Yamada, H., Ohtani, T., Iwanami, A., Aoki, S.,
1348 Kato, N., & Kasai, K. (2009). Smaller amygdala volume and reduced anterior
1349 cingulate gray matter density associated with history of post-traumatic stress
1350 disorder. *Psychiatry Research*, *174*(3), 210–216.
1351 https://doi.org/10.1016/j.pscychresns.2009.06.001

1352 Sagi, Y., Tavor, I., Hofstetter, S., Tzur-Moryosef, S., Blumenfeld-Katzir, T., & Assaf,
1353 Y. (2012). Learning in the fast lane: new insights into neuroplasticity. *Neuron*,
1354 *73*(6), 1195–1203. https://doi.org/10.1016/j.neuron.2012.01.025

1355 Savic, I. (2015). Structural changes of the brain in relation to occupational stress.
1356 *Cerebral Cortex* , *25*(6), 1554–1564. https://doi.org/10.1093/cercor/bht348

1357 Schielzeth, H. (2010). Simple means to improve the interpretability of regression
1358 coefficients. In *Methods in Ecology and Evolution,* 1 (2), 103–113.
1359 https://doi.org/10.1111/j.2041-210x.2010.00012.x

1360 Seeley, W. W. (2019). The Salience Network: A Neural System for Perceiving and
1361 Responding to Homeostatic Demands. *The Journal of Neuroscience: The*
1362 *Official Journal of the Society for Neuroscience*, *39*(50), 9878–9882.
1363 https://doi.org/10.1523/JNEUROSCI.1138-17.2019

1364 Shao, Y., & McCarthy, K. D. (1994). Plasticity of astrocytes. *Glia*, *11*(2), 147–155.
1365 https://doi.org/10.1002/glia.440110209

1366 Spalletta, G., Piras, F., Caltagirone, C., & Fagioli, S. (2014). Hippocampal
1367 multimodal structural changes and subclinical depression in healthy individuals.
1368 *Journal of Affective Disorders*, *152-154*, 105–112.
1369 https://doi.org/10.1016/j.jad.2013.05.068

1370 Streitbürger, D.-P., Möller, H. E., Tittgemeyer, M., Hund-Georgiadis, M., Schroeter,
1371 M. L., & Mueller, K. (2012). Investigating structural brain changes of dehydration
1372 using voxel-based morphometry. *PloS One*, *7*(8), e44195.
1373 https://doi.org/10.1371/journal.pone.0044195

1374 Suffren, S., La Buissonnière-Ariza, V., Tucholka, A., Nassim, M., Séguin, J. R.,

Boivin, M., Kaur Singh, M., Foland-Ross, L. C., Lepore, F., Gotlib, I. H., Tremblay, R. E., & Maheu, F. S. (2021). Prefrontal cortex and amygdala anatomy in youth with persistent levels of harsh parenting practices and subclinical anxiety symptoms over time during childhood. *Development and Psychopathology*, 1–12. https://doi.org/10.1017/S0954579420001716

Tardif, C. L., Steele, C. J., Lampe, L., Bazin, P.-L., Ragert, P., Villringer, A., & Gauthier, C. J. (2017). Investigation of the confounding effects of vasculature and metabolism on computational anatomy studies. *NeuroImage*, *149*, 233–243. https://doi.org/10.1016/j.neuroimage.2017.01.025

Tasker, J. G., & Herman, J. P. (2011). Mechanisms of rapid glucocorticoid feedback inhibition of the hypothalamic-pituitary-adrenal axis. *Stress* , *14*(4), 398–406. https://doi.org/10.3109/10253890.2011.586446

Taubert, M., Mehnert, J., Pleger, B., & Villringer, A. (2016). Rapid and specific gray matter changes in M1 induced by balance training. *NeuroImage*, *133*, 399–407. https://doi.org/10.1016/j.neuroimage.2016.03.017

Thomas, A. G., Dennis, A., Rawlings, N. B., Stagg, C. J., Matthews, L., Morris, M., Kolind, S. H., Foxley, S., Jenkinson, M., Nichols, T. E., Dawes, H., Bandettini, P. A., & Johansen-Berg, H. (2016). Multi-modal characterization of rapid anterior hippocampal volume increase associated with aerobic exercise. *NeuroImage*, *131*, 162–170. https://doi.org/10.1016/j.neuroimage.2015.10.090

Thomas, C., Sadeghi, N., Nayak, A., Trefler, A., Sarlls, J., Baker, C. I., & Pierpaoli, C. (2018). Impact of time-of-day on diffusivity measures of brain tissue derived from diffusion tensor imaging. *NeuroImage*, *173*, 25–34. https://doi.org/10.1016/j.neuroimage.2018.02.026

Trefler, A., Sadeghi, N., Thomas, A. G., Pierpaoli, C., Baker, C. I., & Thomas, C. (2016). Impact of time-of-day on brain morphometric measures derived from T1-weighted magnetic resonance imaging. *NeuroImage*, *133*, 41–52. https://doi.org/10.1016/j.neuroimage.2016.02.034

Tsigos, C., & Chrousos, G. P. (2002). Hypothalamic-pituitary-adrenal axis, neuroendocrine factors and stress. *Journal of Psychosomatic Research*, *53*(4), 865–871. https://doi.org/10.1016/s0022-3999(02)00429-4

Tynan, R. J., Beynon, S. B., Hinwood, M., Johnson, S. J., Nilsson, M., Woods, J. J., & Walker, F. R. (2013). Chronic stress-induced disruption of the astrocyte network is driven by structural atrophy and not loss of astrocytes. *Acta Neuropathologica,* 126(1), 75–91. https://doi.org/10.1007/s00401-013-1102-0

Van Cauter, E., & Refetoff, S. (1985). Evidence for Two Subtypes of Cushing's Disease Based on the Analysis of Episodic Cortisol Secretion. *New England Journal of Medicine,* 312 (21), 1343–1349. https://doi.org/10.1056/nejm198505233122102

Veer, I. M., Oei, N. Y. L., Spinhoven, P., van Buchem, M. A., Elzinga, B. M., & Rombouts, S. A. R. B. (2011). Beyond acute social stress: increased functional connectivity between amygdala and cortical midline structures. *NeuroImage*, *57*(4), 1534–1541. https://doi.org/10.1016/j.neuroimage.2011.05.074

Veer, I. M., Oei, N. Y. L., Spinhoven, P., van Buchem, M. A., Elzinga, B. M., & Rombouts, S. A. R. B. (2012). Endogenous cortisol is associated with functional connectivity between the amygdala and medial prefrontal cortex. *Psychoneuroendocrinology*, *37*(7), 1039–1047. https://doi.org/10.1016/j.psyneuen.2011.12.001

Vining, R. F., McGinley, R. A., Maksvytis, J. J., & Ho, K. Y. (1983). Salivary cortisol: a better measure of adrenal cortical function than serum cortisol. *Annals of Clinical Biochemistry*, *20 (Pt 6)*, 329–335. https://doi.org/10.1177/000456328302000601

Wang, J., Rao, H., Wetmore, G. S., Furlan, P. M., Korczykowski, M., Dinges, D. F., & Detre, J. A. (2005). Perfusion functional MRI reveals cerebral blood flow pattern under psychological stress. *Proceedings of the National Academy of Sciences of the United States of America*, *102*(49), 17804–17809. https://doi.org/10.1073/pnas.0503082102

Wheelock, M. D., Harnett, N. G., Wood, K. H., Orem, T. R., Granger, D. A., Mrug, S., & Knight, D. C. (2016). Prefrontal Cortex Activity Is Associated with Biobehavioral Components of the Stress Response. *Frontiers in Human Neuroscience*, *10*, 583. https://doi.org/10.3389/fnhum.2016.00583

Wickham, H. (2009). *ggplot2: Elegant Graphics for Data Analysis*. Springer Science & Business Media. https://play.google.com/store/books/details?id=bes-

AAAAQBAJ

Wright, P. J., Mougin, O. E., Totman, J. J., Peters, A. M., Brookes, M. J., Coxon, R., Morris, P. E., Clemence, M., Francis, S. T., Bowtell, R. W., & Gowland, P. A. (2008). Water proton T 1 measurements in brain tissue at 7, 3, and 1.5T using IR-EPI, IR-TSE, and MPRAGE: results and optimization. *Magnetic Resonance Materials in Physics, Biology and Medicine,* 21 (1-2), 121–130. https://doi.org/10.1007/s10334-008-0104-8

Zatorre, R. J., Fields, R. D., & Johansen-Berg, H. (2012). Plasticity in gray and white: neuroimaging changes in brain structure during learning. *Nature Neuroscience*, *15*(4), 528–536. https://doi.org/10.1038/nn.3045